Assimilation of IASI Ozone-Sensitive Channels in Preparation for an Enhanced Coupling Between Numerical Weather Prediction and Chemistry Transport Models

Olivier Coopmann, V. Guidard, Nadia Fourrié, Matthieu Plu

AGU100 ADVANCING EARTH AND SPACE SCIENCE

JGR

Journal of Geophysical Research: Atmospheres

RESEARCH ARTICLE
10.1029/2017JD027901

Key Points:
- IASI ozone-sensitive channels are also sensitive to temperature and humidity
- Using a realistic ozone information input of the RTTOV RTM allows to better simulate IASI ozone-sensitive channels radiances
- A simplified framework such as the 1D-Var data assimilation is used to prepare for an enhanced coupling between NWP and CTM

Correspondence to:
O. Coopmann,
olivier.coopmann@umr-cnrm.fr

Citation:
Coopmann, O., Guidard, V., Fourrié, N., & Plu, M. (2018). Assimilation of IASI ozone-sensitive channels in preparation for an enhanced coupling between Numerical Weather Prediction and Chemistry Transport Models. *Journal of Geophysical Research: Atmospheres*, *123*, 12,452–12,473. https://doi.org/10.1029/2017JD027901

Received 17 OCT 2017
Accepted 4 OCT 2018
Accepted article online 25 OCT 2018
Published online 10 NOV 2018

Assimilation of IASI Ozone-Sensitive Channels in Preparation for an Enhanced Coupling Between Numerical Weather Prediction and Chemistry Transport Models

O. Coopmann[1], **V. Guidard**[1], **N. Fourrié**[1], **and M. Plu**[1]

[1]CNRM, Université de Toulouse, Météo-France, CNRS, Toulouse, France

Abstract In this study, IASI ozone-sensitive channels have been assimilated in 1D-Var data assimilation combined with realistic ozone background coming from a MOCAGE (Modèle de Chimie Atmosphérique à Grande Echelle) Chemistry Transport Model (CTM) as a first stage of coupling between Numerical Weather Prediction (NWP) and MOCAGE CTM at Météo-France for global model ARPEGE (Action de Recherche Petite Echelle Grande Echelle). To evaluate the impact of ozone-sensitive channels on analyses, databases of 161 temperatures, humidity, and ozone radiosondes across the globe during a 1-year period have been considered. Ozone forecast from MOCAGE CTM was evaluated with radiosondes and used as input for the Radiative Transfer Model (RTM) RTTOV. Statistics of IASI observations minus simulations show that the use of ozone from MOCAGE CTM allows to better simulate IASI ozone-sensitive channels. The Desroziers method is used to diagnose observation error covariance matrix and estimate realistic ozone observation standard errors taking into account cross-correlations between IASI channels. The background error covariance matrix for ozone is estimated using radiosondes. A control run assimilating 123 IASI operational channels is compared to an experiment which assimilates, in addition, 15 IASI ozone-sensitive channels. Results show potential benefits of IASI ozone-sensitive channels combined with realistic ozone from MOCAGE CTM to improve temperature, humidity and ozone analyses simultaneously. This work is an encouraging first step for the enhancing of the coupling between the global model ARPEGE and MOCAGE CTM.

1. Introduction

Since the launch in 1960 of the first weather satellite, techniques have significantly evolved with ever more sophisticated instruments. Data from space borne instruments that are assimilated in Numerical Weather Prediction (NWP) systems have a positive impact on forecasts (Lorenc & Marriott, 2014). IASI (Infrared Atmospheric Sounding Interferometer) was jointly developed by CNES (Centre National d'Études Spatiales) and EUMETSAT (European Organisation for the Exploitation of Meteorological Satellites; Cayla, 2001). It was first launched in 2006 onboard the Metop-A satellite. The second instrument was launched on board Metop-B in 2012 and its spectrum ranges from 645 to 2,760 cm^{-1} with a spectral sampling of 0.25 cm^{-1} and a spectral resolution of 0.5 cm^{-1} leading to a set of 8,461 radiance measurements. This sounder provides indirect information on temperature and humidity profiles to be obtained along with that of cloud cover, aerosols, atmospheric chemistry compounds such as O_3, CO_2, CO, CH_4, HNO_3, and N_2O (Clerbaux et al., 2009) and surface properties. The retrieval precision aimed for is 1 K/1 km in terms of temperature and 10%/1 km in terms of humidity (Hilton et al., 2012). This accuracy in temperature retrievals is achieved over oceans but is more challenging over land and near to the surface due for example to weaker instrument sensitivity combined with larger uncertainties especially on input surface parameters skin temperature (Guedj et al., 2011) and emissivity. (Guedj et al., 2011) was interested in land surface temperature retrievals in order to improve the assimilation of SEVIRI radiances.

The high volume of data resulting from IASI presents many challenges, particularly in the areas of data transmission, data storage and assimilation for example. The methods for reducing the data volume are channel selection, spatial sampling or principle components analysis. A channel selection was performed by (Collard, 2007) for NWP purposes. Channels were mainly selected in the CO_2 longwave (LW) band (for temperature retrievals), in the atmospheric window region and in the water vapor (WV) band. This selection of 300 channels includes 15 ozone-sensitive channels. CNES added 14 other channels for climate monitoring purposes.

Table 1
Number and Wave Number of the 15 Ozone-Sensitive IASI Channels Available in the Météo-France 314 Channel Subset

Channel number	Wave number (cm^{-1})	Channel number	Wave number (cm^{-1})	Channel number	Wave number (cm^{-1})
1479	1,014.50	1574	1,038.25	1639	1,054.50
1509	1,022.00	1579	1,039.50	1643	1,055.50
1513	1,023.00	1585	1,041.00	1652	1,057.75
1521	1,025.00	1587	1,041.50	1658	1,059.25
1536	1,028.75	1626	1,051.25	1671	1,062.50

This subset of 314 channels including Collard's selection is routinely monitored at Météo-France and up to 123 channels are assimilated in operations (99 temperature channels in the LW CO_2 band, 4 window channels and 20 WV channels). IASI-A and IASI-B alone account for 58% of the data used in the NWP global model ARPEGE (Action de Recherche Petite Echelle Grande Echelle) of Météo-France. The Global Telecommunication System also distributes a set of 500 channels (Martinet et al., 2014), which includes the 314-channels subset.

IASI ozone-sensitive channels are potentially beneficial because they are also sensitive to temperature and humidity and can therefore provide additional information for 4D-Var (four-dimensional variational data assimilation) data assimilation. Indeed, the work of Derber and Wu (1998) showed that realistic ozone information improves the use of ozone-sensitive channel satellite radiances in the High Infrared Resolution Sounder (HIRS) at the global forecast system at NCEP (National Centers for Environmental Prediction). Semane et al. (2009) showed potential benefits of 4D-Var ozone assimilation for the improvement of the wind field through dynamics-ozone coupling at the global model ARPEGE. Many more studies have shown the benefits of ozone assimilation for NWP. ECMWF's (European Centre for Medium-Range Weather Forecasts) Integrated Forecasting System (IFS) assimilates 16 IASI ozone-sensitive channels (in their own channel subset) in operational near-real-time providing ozone analysis (Dragani & McNally, 2013; Han & McNally, 2010). Lupu and McNally (2013) have shown through their study the positive impact on wind analysis assimilating ozone-sensitive channels from the Spinning Enhanced Visible and Infrared Imager (SEVIRI) instrument. These studies only assessed impact on wind and not on temperature and humidity forecast however. Additionally, IASI radiances may be used to provide Level 2 products such as temperature and humidity profiles, cloud information, surface emissivity and temperature, and atmospheric composition in near-real time. IASI operational Level 2 products from EUMETSAT version 5 algorithm are coretrieving temperature and ozone profiles (August et al., 2012). At present, Météo-France does not use these L2 products, only L1 products (radiances).

MOCAGE (Modèle de Chimie Atmosphérique à Grande Echelle) Chemistry Transport Model (CTM) is a three-dimensional CTM of the troposphere and stratosphere providing a realistic ozone background at Météo-France. This background is consistent with dynamical fields of the global model ARPEGE as MOCAGE is piloted by ARPEGE dynamics.

The present study is a preparatory study so as to demonstrate the potential benefits of extracting information from 15 IASI ozone-sensitive channels monitored at Météo-France. This is done by using realistic ozone background to simultaneously improve temperature, humidity and ozone analyses. A 1D-Var assimilation framework is used and this paper is outlined as follows: Section 2 describes the data sets used in this study, IASI ozone-sensitive channels, thermodynamics and ozone information and radiosondes, section 3 evaluates the impact of ozone background input on a Radiative Transfer Model (RTM) simulation of radiances, and section 4 presents the assimilation setup and observation and background errors used. The results of 1D-Var assimilation are shown in section 5. Finally, section 6 summarizes the results and opens discussion.

2. Description of the Data Sets

2.1. IASI Observations

IASI is a Michelson interferometer measuring infrared. It measures 8,461 spectral samples between 3.62 and 15.5 μm with a resolution of 0.5 cm^{-1} after apodization. IASI scans across-track in 30 successive elementary fields of view (EFOVs), each composed of four instantaneous fields of view (IFOV). The EFOV's span a ±48.33° range, symmetric with respect to the Nadir, in steps of 3.33°. The swath width on the ground is approximately 2200 km, which provides global Earth coverage twice a day. The IFOV is a disc of 12 km (pixel) diameter at

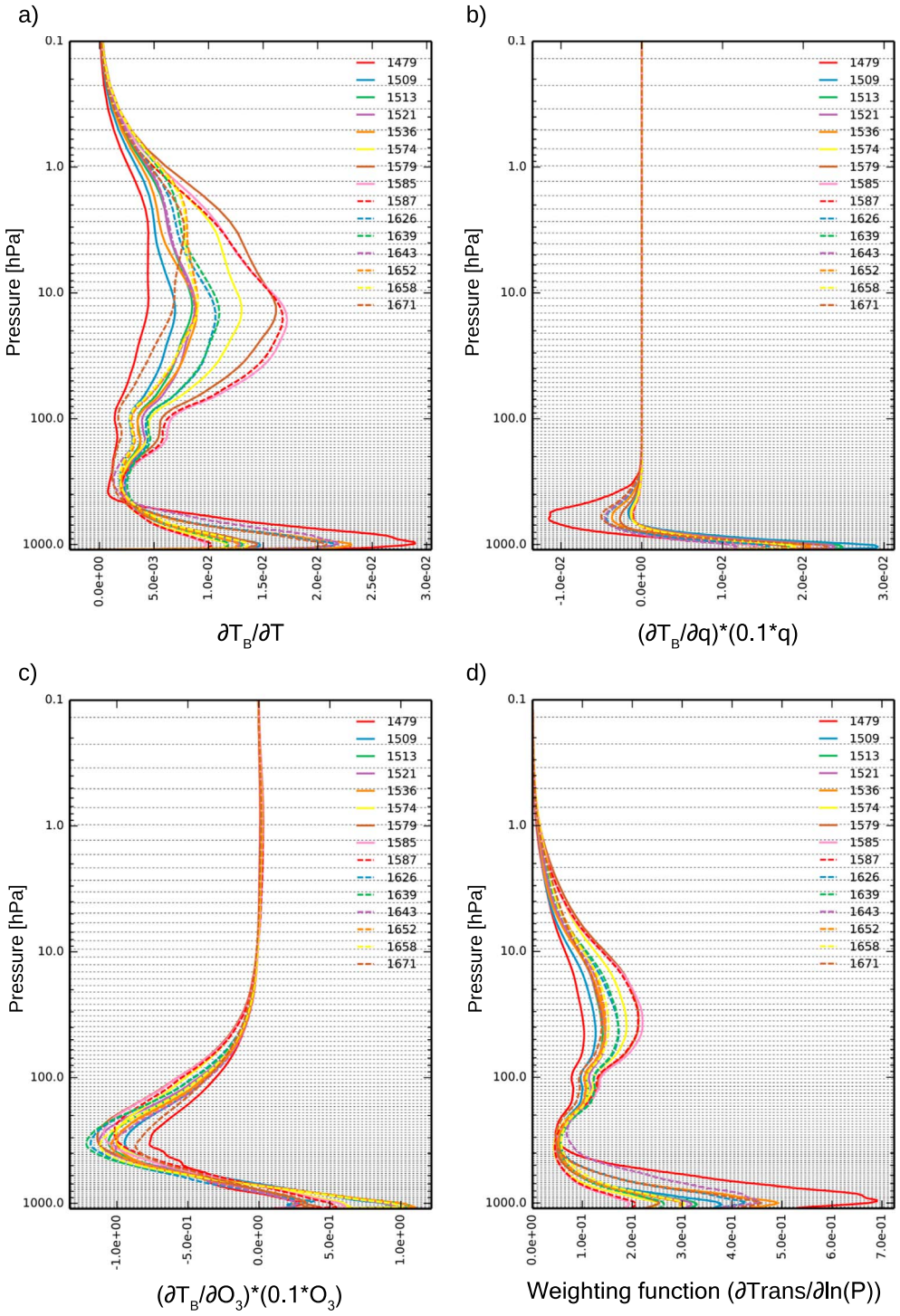

Figure 1. Jacobians of temperature (a), humidity (b), ozone (c), and weighting functions (d) for 15 IASI ozone-sensitive channels using O3REF profile.

subsatellite point (August et al., 2012). Operationally at Météo-France, 314 IASI channels are monitored and 123 are assimilated: 99 CO_2 sensitive channels in the LW to retrieve temperature profiles, 4 window channels, and 20 H_2O sensitive channels in the LW to retrieve humidity profiles. The 15 IASI ozone-sensitive channels that are monitored range from 1014.5 to 1062.5 cm^{-1} (Table 1).

We have evaluated the sensitivity of these channels to temperature, humidity and ozone by computing their Jacobians (Figures 1a–1c). The Jacobian represents the sensitivity of brightness temperature with respect to

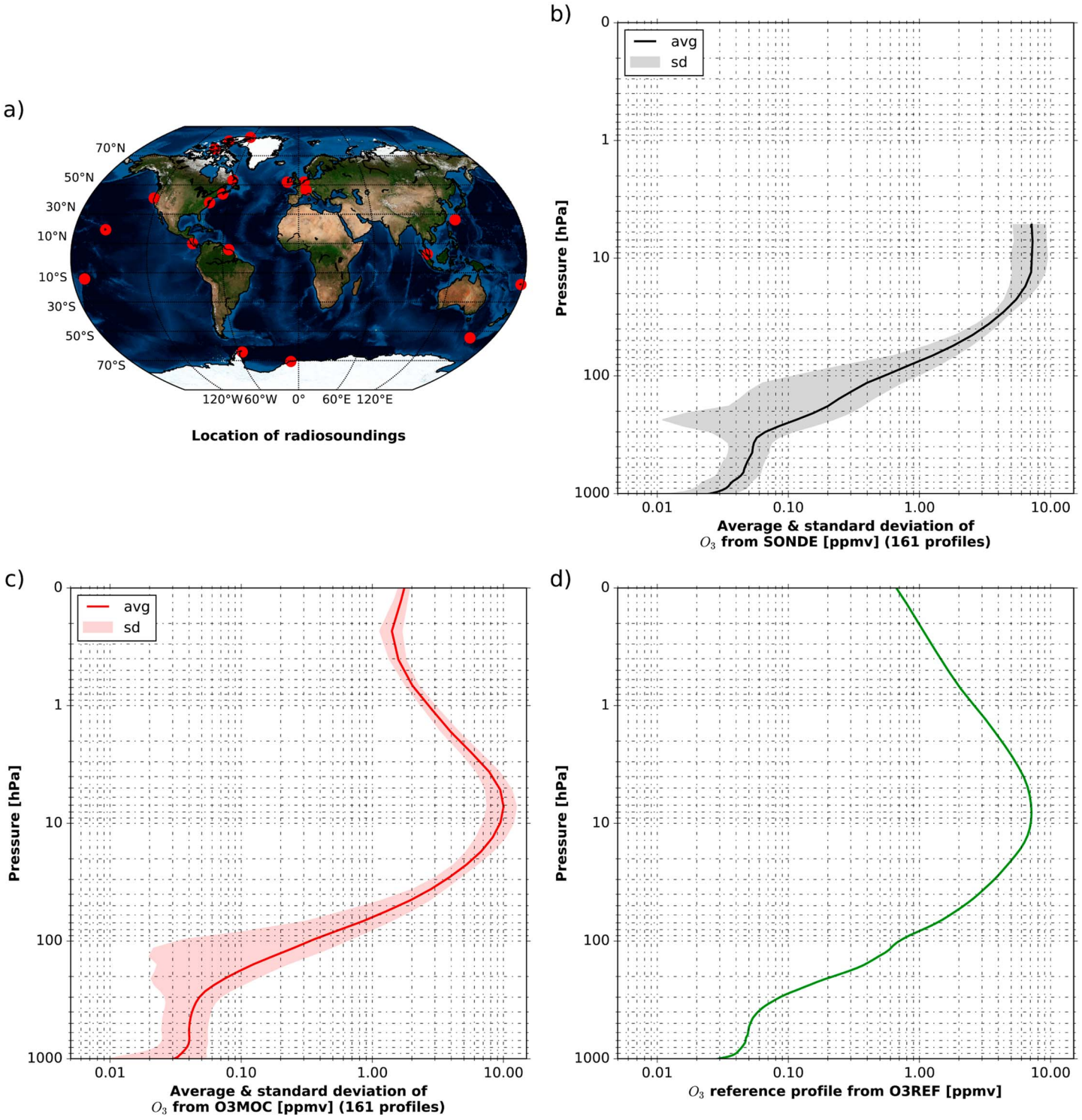

Figure 2. Location of radiosoundings from (WOUDC, SHADOZ, and NOAA) networks used in this study (a), average and standard deviation of the 161 ozone profiles from SONDE (b), O3MOC (c), and ozone reference profile from O3REF (d) with respect to pressure.

a change in thermodynamic or chemical parameters. Jacobians for temperature (T), humidity (q), and ozone (O_3) have been calculated with an average profile coming from RTTOV RTM data sets. Jacobians of humidity and ozone have been multiplied by 10% of their concentrations to overcome the large variability of these parameters. Temperature Jacobians (Figure 1a) for the 15 ozone-sensitive channels show broader values in the lower troposphere (1,000–500 hPa) with a peak around $0.03K.K^{-1}$ and in the large part of the stratosphere (100–1 hPa) with a peak around $0.015K.K^{-1}$. In Figure 1b, humidity Jacobians show the largest values in the lower troposphere between 1,000 and 900 hPa with a peak around $0.03K$ and in the middle troposphere (800–300 hPa) with a peak around $0.01K$. In Figure 1c, ozone Jacobians then show large values in the lower troposphere (1,000–800 hPa) and in the middle troposphere up to the lower stratosphere (700–30 hPa) with peaks around $\pm 1.0K$. In addition, Figure 1d present the weighting functions of these ozone-sensitive channels, that is, the derivative of the atmospheric transmission profile with respect to the vertical coordinate. Weighting functions show peaks of sensitivity at several altitudes (lower troposphere and stratosphere). These results show the interest in using IASI ozone-sensitive channels for NWP because these channels are also sensitive to temperature and humidity and could potentially provide further information in the data assimilation process.

2.2. Collocation Between Radiosondes and IASI Pixels

In this section, data sets used in the study are described. A 1-year period from April 2014 to March 2015 was selected to take into account the annual variability. Before the collocation between radiosondes and IASI pixels, we were starting from a set of 1,767 radiosounding profiles launched from 50 stations. Temperature, humidity, and ozone data were measured using radiosondes from the collection of

- the World Ozone and Ultraviolet Data Center (WOUDC, available online at http://www.woudc.org);
- the Southern Hemisphere Additional Ozonesondes (SHADOZ, available online at croc.gsfc.nasa.gov/shadoz/Archive.html); and
- the National Oceanic and Atmospheric Administration (NOAA)/Earth System Research Laboratory (ESRL), Global Monitoring Division (GMD) networks (available online at ftp://ftp.cmdl.noaa.gov/ozwv/ozone/).

After screening to remove erroneous profiles (missing or/and spurious data), we were left with data from 49 stations with a set of 1,688 radiosounding profiles. It is important to note that the radiosondes, named SONDE hereafter, provide a sufficient amount of data only up to 10 hPa. In addition, these radiosondes are not assimilated in the 4D-Var global model ARPEGE.

In order to collocate IASI pixels and radiosondes, several criteria were defined so as to select the closest pixel for each radiosonde. The smallest orthodromic distance and temporal difference between IASI pixel and radiosonde were retained. Only the IASI pixels nearest radiosonde were selected from those within an orthodromic distance below 150 km and a temporal difference below 60 min. The IASI instrument also includes an Integrated Imaging Subsystem (IIS) that allows to coregister interferometric measurements with AVHRR (Advanced Very High Resolution Radiometer), present on the same platform. AVHRR provides cloud and heterogeneity information in the IASI pixels (Saunders & Kriebel, 1988). To avoid the use of cloudy pixels, IASI pixels were discarded whenever the AVHRR cloud cover was above 15%. To avoid emissivity and surface temperature problem, only pixels over sea with less than 10% of land fraction were retained. Indeed, sea surface temperatures are known to be more accurate (around 0.5 K; Donlon et al., 2012 than land surface temperatures (few Kelvin), and the RTTOV RTM includes a surface emissivity model (ISEM; Sherlock & Saunders, 1999) over the sea while only an atlas is available over land (Borbas & Ruston, 2011). Finally, profiles with a difference between simulated IASI observation and real IASI observation (named innovation or first guess departure) larger than (in absolute value) 5 K were rejected. Indeed, large innovations could result from the presence of a cloud or a wrong surface description hence the 161 remaining pixels collocated with radiosounding profiles, among the 1,688 starting data, were used in the following study. In situ temperature, humidity, and ozone profiles from these radiosoundings have been used as verification data. Average and standard deviation of 161 ozone profiles (23 stations shown in Figure 2a) from SONDE are given in Figure 2b with respect to pressure.

2.3. Model Atmospheric Data

The first source of information for ozone emanates from O3REF (Matricardi, 2008), which is constant in time and space with 101 levels up to 0.005 hPa and used operationally at Météo-France (Figure 2d). This profile results from averaging a set of 83 diverse profiles from ECMWF analyses on 91 levels, interpolated in to 101 levels (Chevallier et al., 2006).

The second source of information for ozone available at Météo-France (every 3 hr) is an ozone realistic field from the model MOCAGE (O3MOC) which has 60 vertical hybrid sigma-pressure levels from the surface up to

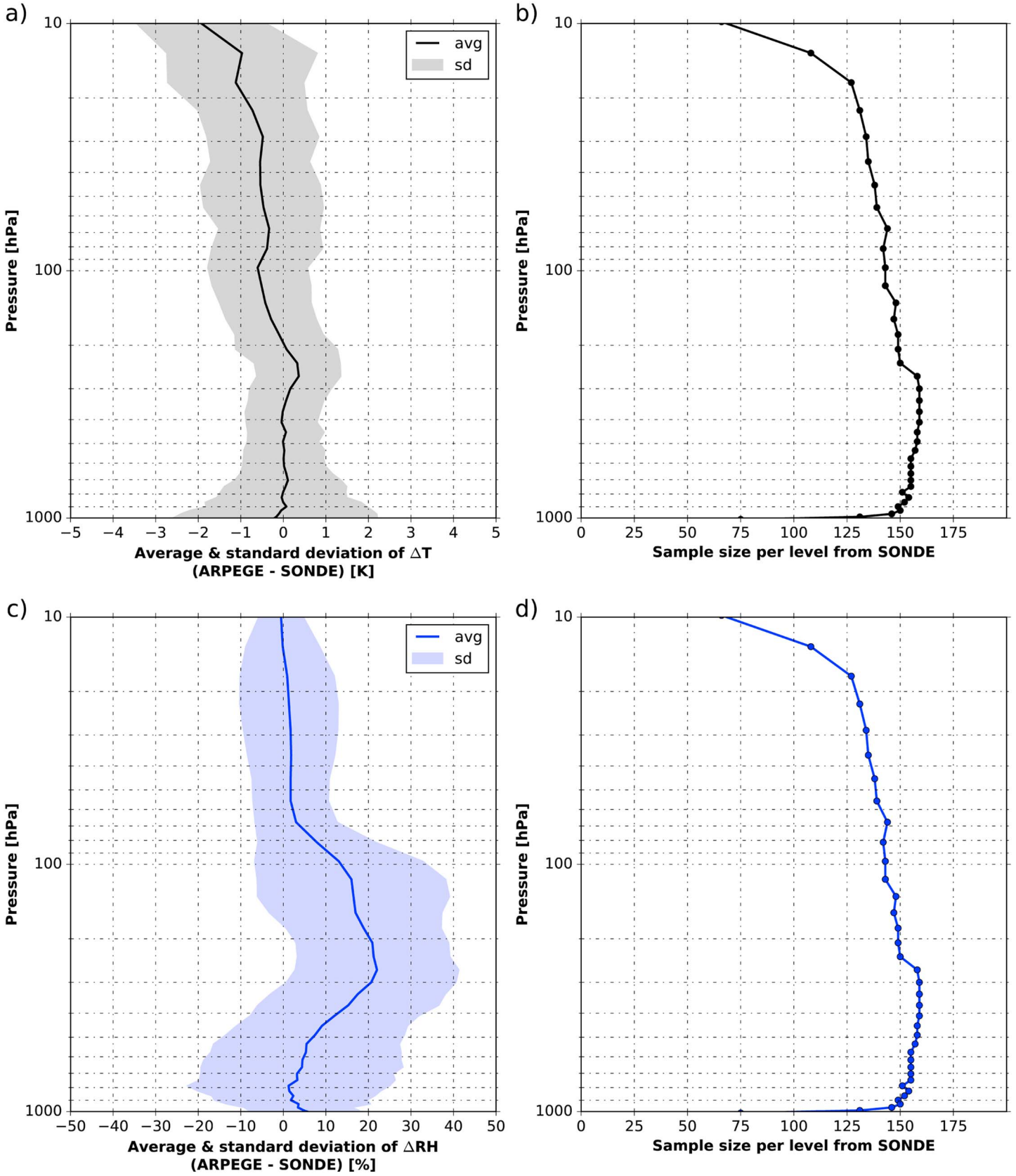

Figure 3. Average and standard deviation of differences between ARPEGE minus SONDE for temperature (a) and relative humidity (c) with respect to pressure and sample size per level for temperature (b) and relative humidity (d).

about 0.01 hPa and which takes into account the atmospheric chemical reactions describing the sources and sinks in time and space on a 2° global grid. The dynamics within the CTM are forced by ARPEGE meteorological analysis fields (pressure, winds, temperature, specific humidity; Sic et al., 2015.

The atmospheric profiles of temperature, specific humidity and surface parameters (skin temperature, surface temperature, surface humidity, surface pressure, zonal wind, and meridian wind) come from the global model ARPEGE forecasts (every 3 hr), which have been extracted for the same period and location as for the radiosondes as well as ozone profiles stemming from MOCAGE. Pressure levels of thermodynamics profiles (70 levels in ARPEGE at the time of the study case), ozone profiles from O3MOC (60 levels) and ozone reference profile from O3REF, were interpolated onto the 54 levels of the 1D-Var from the NWP-SAF (Numerical Weather Prediction Satellite Application Facility) of Eumetsat (http://nwpsaf.eu/site/software/1d-var). In Figure 2c, we show average and standard deviation of 161 ozone profiles from O3MOC with respect to pressure.

2.3.1. Statistics on Thermodynamic Profiles

To evaluate the 161 thermodynamic profiles, statistics between temperature and humidity from the forecasts of ARPEGE minus radiosondes (SONDE), were calculated between 1,013 and 5 hPa, across 40 pressure bins, relatively evenly spaced on a logarithmic scale. In Figure 3a, temperature bias between ARPEGE and SONDE of −0.25 K is observed at the surface with a standard deviation of around 2.5 K. This may be due to the surface temperature over sea ice, which is not simulated by the ARPEGE model (i.e., prescribed climatological values) over high latitudes. Additionally, the radiosoundings launched close to the coastal areas have very variable surface temperatures while the profiles extracted from the model only take into account the sea surface temperature. We note a temperature bias less than ±0.75 K between 950 and 30 hPa with standard deviation around 1.0 K. Then higher biases above 30 hPa are also noted for temperatures with increasing standard deviation, probably due to the decrease of the number of SONDE data, especially above 20 hPa. Figure 3b shows relative humidity biases between ARPEGE and SONDE. A positive bias of 0.5% is observed at the surface with a standard deviation of around 10%. Between the surface and 800 hPa, the bias decreases to 2% while the standard deviation increases by up to 25%. Then we note a positive bias of up to 20% between 800 and 70 hPa with standard deviation ranging from 10% and 20%. Finally, relative humidity biases are close to 0% above 70 hPa with a standard deviation of around 10%.

The expected accuracy of IASI retrievals for temperature (1 K/1 km) is already achieved in the model forecast to be used as prior information in the retrieval process in large parts of the atmosphere, but not near the surface, as previously explained, due probably to the surface temperature over sea ice. The standard deviation of humidity is however larger than 10%/1 km in the whole troposphere, showing that the vertical variations of humidity are difficult to model but also due to differences between model and the sonde, which are not exactly collocated and have different horizontal scales. The choice of prior information for humidity is very important as it is very difficult to correct errors in the vertical structure of the humidity profile using data assimilation methods (Hilton et al., 2009; Pougatchev et al., 2009).

2.3.2. Statistics on Ozone Profiles

Similar features in terms of biases and standard deviations are noticed with 161 profiles from O3MOC (see Figure 4a). We note that O3MOC overestimates ozone between 300 and 20 hPa around 0.1 up to 0.6 ppmv with standard deviation increasing (0.5 ppmv) up to 10 hPa, and underestimating it above 20 hPa. The biases of ozone from O3REF with respect to SONDE behave differently compared with O3MOC. Indeed, in Figure 4b, O3REF underestimates ozone between 300 and 40 hPa and overestimates it above 40 hPa with a large standard deviation (2 ppmv). These results were expected and confirm that ozone from O3MOC better describes the variability of ozone than the constant ozone profile from O3REF.

3. Sensitivity of Simulations to Ozone Information

To extract further information stemming from IASI observations, we need to confront the observations with what the model already knows. For this purpose, simulations of IASI observations are obtained with a RTM known as RTTOV at Météo-France. RTTOV (Radiative Transfer for TOVS; TOVS: TIROS Operational Vertical Sounder and TIROS: Television Infrared Observation Satellite; RTTOV v11 Users Guide, NWPSAF-MO-US-028; Saunders et al., 1999) is a RTM developed in the framework of the NWP-SAF of EUMETSAT (http://nwpsaf.eu/site/software/rttov) to meet the demands of operational data assimilation systems from national weather services. RTTOV simulates the top of the atmosphere clear-sky radiances in the visible, infrared and microwave for each available channel. RTTOV also has the capability to simulate the cloud and aerosol scattering. Simulated

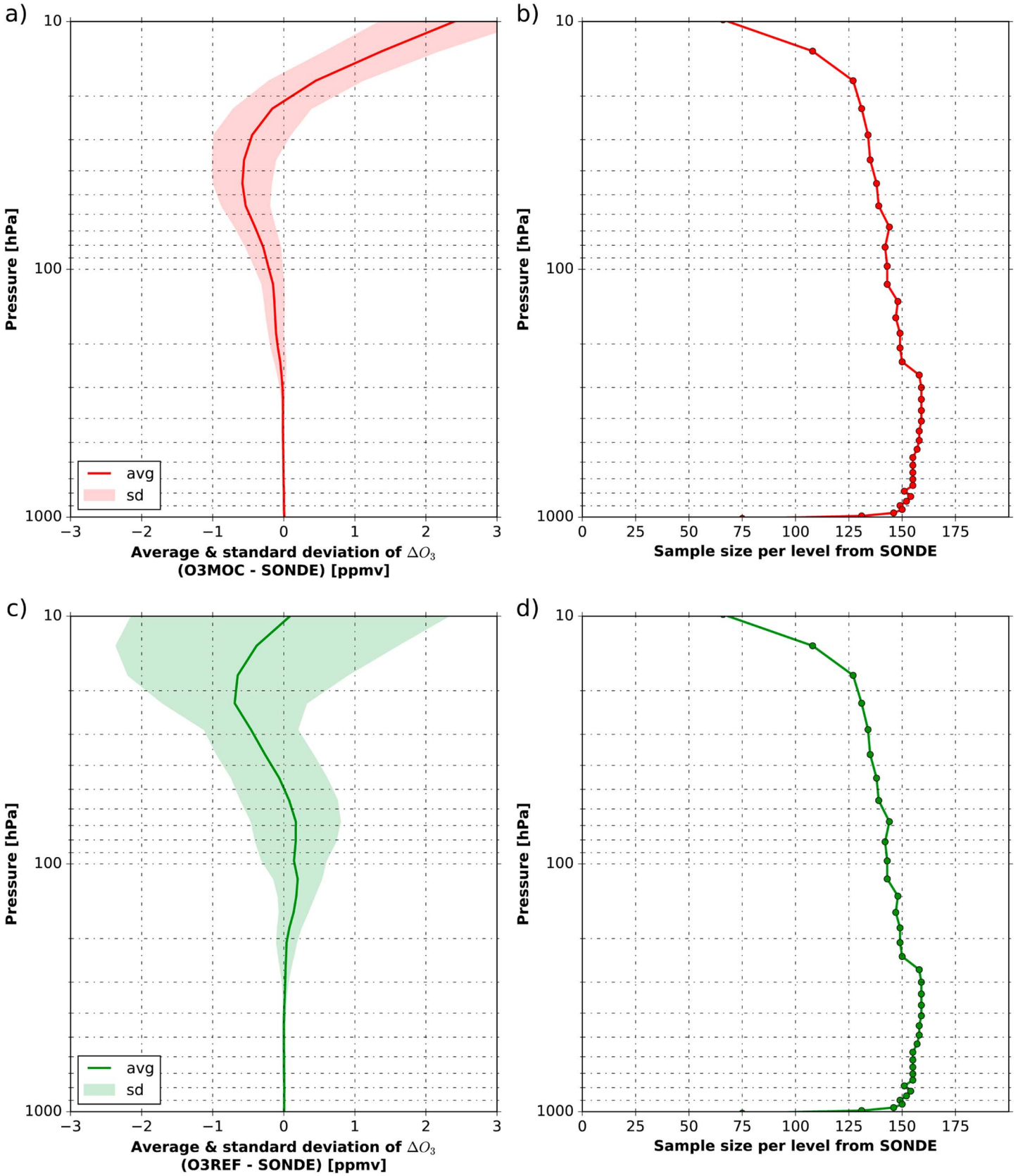

Figure 4. Average and standard deviation of ozone differences between O3MOC minus SONDE (a) and O3REF minus SONDE (c) with respect to pressure and sample size per level for O3MOC (b) and O3REF (d).

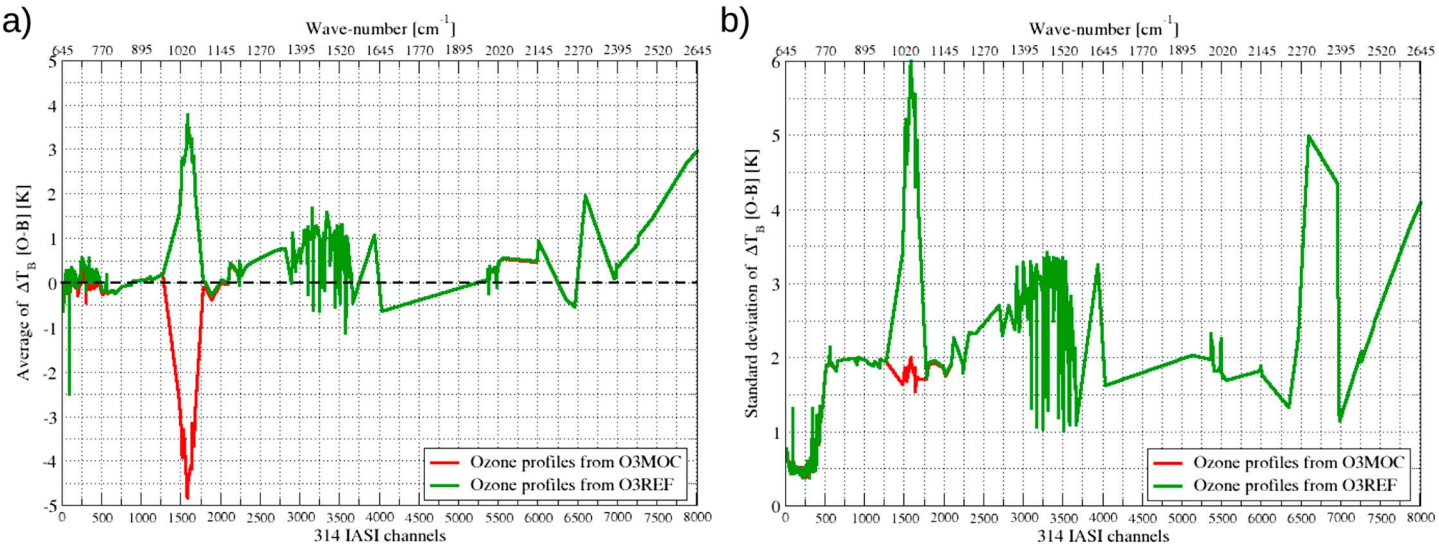

Figure 5. Average (a) and standard deviation (b) of brightness temperature (T_B) differences between real observations and simulations [O-B] with O3REF (green line) and O3MOC (red line) ozone fields for 314 IASI channels with respect to wave numbers.

IASI observations are then compared to real IASI observations. The sensitivity of brightness temperature simulations to both O3REF and O3MOC ozone profiles is assessed in this part. In order to initialize the RTM, we use the 161 temperatures, humidity profiles and surface parameters from ARPEGE. The only difference between experiments is in the ozone profiles. RTM provides 161 simulations of IASI observations for 314 channels which are then compared to 161 real IASI observations. Average and standard deviations of brightness temperature differences between IASI observations and simulations [O-B], where [O-B] represents the innovation, are displayed in Figure 5.

Differences are mainly located in the ozone band between 1014.5 and 1062.5 cm^{-1} as expected. A bias for O3MOC with values around −5 K is observed in Figure 5a. On the other hand, the O3REF ozone bias remains lower than O3MOC, around 3.5 K. A similar bias has been observed for O3MOC whatever the region, while bias for O3REF is more variable by region ranging from −1 K in the Polar region to 11 K in the Tropics (not shown). These results are consistent with large biases of O3MOC above 15 hPa compared with O3REF seen in Figure 4. These values were used to carry out bias correction of IASI observations for assimilation experiments. Some CO_2 channels appear to be sensitive to ozone between 650 and 800cm^{-1}. We observed in Figure 5b a large standard deviation of [O-B] brightness temperature differences for the IASI ozone sensitive-channels using ozone information from O3REF with values up to 6 K. The use of realistic ozone information from O3MOC leads however to the reduction of standard deviation of around 1.75 K for ozone-sensitive channels. Inaccurate skin temperature and the sea-ice over high latitudes may lead to higher standard deviations in window regions. Standard deviation of [O-B] brightness temperature differences using ozone information from O3MOC are an indication that the variable ozone profiles of O3MOC allow to better simulate IASI radiances than do O3REF. These results are expected and are consistent with the statistics on ozone profiles in section 2.3.2 with a larger bias of O3MOC than O3REF, but standard deviation is twice larger using O3REF than O3MOC in the stratosphere.

4. Experimental Method

4.1. Formalism of Data Assimilation

Data assimilation allows the best estimate $\mathbf{x}^a$ of the real state of the atmosphere to be found from observations $\mathbf{y}$ and a prior knowledge of the atmosphere (the background) $\mathbf{x}^b$, which is usually a short-term forecast. The errors of these two sources of information should be unbiased (zero mean). In a one-dimensional framework, atmospheric thermodynamic profiles at a given location are represented by a vector $\mathbf{x}$ and satellite radiances or brightness temperatures by a vector $\mathbf{y}$. Differences between observations and simulated observations formulated as $\mathbf{d}_b^o = \mathbf{y} - \mathcal{H}(\mathbf{x}^b)$ are known as innovations. The transition from background model space to observation space is realized by the observation operator $\mathcal{H}$, which simulates brightness temperatures from $\mathbf{x}^b$ through the RTM. It can include horizontal and vertical interpolation.

Additionally, the following errors must be taken into account: the background error $\varepsilon^b = \mathbf{x}^b - \mathbf{x}^t$ and the observation error $\varepsilon^o = \mathbf{y} - \mathcal{H}(\mathbf{x}^t) = (\mathbf{y} - \mathbf{y}^t) + (\mathbf{y}^t - \mathcal{H}(\mathbf{x}^t)) = \varepsilon^i + \varepsilon^f$, where $\mathbf{x}^t$ is the truth in the model space, $\mathbf{y}^t$ is the truth in the observation space, ε^i is the error due to instrument noise, and ε^f is the error in the observation operator and the representativeness error, which is induced by the difference of scale between the observation and the model.

In addition, the background-error covariance matrix is defined as $\mathbf{B} = E(\varepsilon^b \varepsilon^{bT})$ and the observation-error covariance matrix: $\mathbf{R} = E(\varepsilon^o \varepsilon^{oT})$, where E stands for the mathematical expectation. The background and observation error covariance matrices determine how much weight should be given to each source of information. The background-error covariance matrix contributes to filtering and propagating the innovation (Bouttier & Kelly, 2001).

A One-Dimensional Variational data assimilation (1D-Var) software developed within the frame of the EUMETSAT NWP SAF is used in this study. The purpose is to estimate the most likely atmospheric state $\mathbf{x}^a$ using observations $\mathbf{y}$ and short range forecasts $\mathbf{x}^b$, in accordance with their respective errors. The analysis state $\mathbf{x}^a$ minimizes the cost function J:

$$J(\mathbf{x}) = \underbrace{\frac{1}{2}\left(\mathbf{x}^b - \mathbf{x}\right)^T \mathbf{B}^{-1} \left(\mathbf{x}^b - \mathbf{x}\right)}_{J_b(x)} + \underbrace{\frac{1}{2}(\mathbf{y} - \mathcal{H}(\mathbf{x}))^T \mathbf{R}^{-1} (\mathbf{y} - \mathcal{H}(\mathbf{x}))}_{J_o(x)}$$

where J_b is the background term and J_o is the observation term.

The analysis state $\mathbf{x}^a$ can be written:

$$\mathbf{x}^a = \mathbf{x}^b + \mathbf{K}\left(\mathbf{y} - \mathcal{H}(\mathbf{x}^b)\right)$$

where the linear operator (Kalman gain matrix) $\mathbf{K} = \mathbf{B}\mathbf{H}^T(\mathbf{H}\mathbf{B}\mathbf{H}^T + \mathbf{R})^{-1} = \mathbf{A}\mathbf{H}^T\mathbf{R}^{-1}$ and $\mathbf{A}$ is the analysis-error covariance matrix $\mathbf{A} = (\mathbf{B}^{-1} + \mathbf{H}^T\mathbf{R}^{-1}\mathbf{H})^{-1} = (\mathbf{I} - \mathbf{K}\mathbf{H})\mathbf{B}$, where $\mathbf{I}$ is the identity matrix. The analysis $\mathbf{x}^a$ is obtained as $\mathbf{x}^a = \mathbf{x}^b + \delta\mathbf{x}^a$ where $\delta\mathbf{x}^a$ is the analysis increment.

4.2. Background Errors

The background-error covariance matrix $\tilde{\mathbf{B}}$ was computed for 1D-Var experiments for 161 profiles. Generally, temperature, humidity, skin temperature, surface temperature and surface humidity are in the 1D-Var control variable. Here, we have also carried out a 1D-Var experiment including ozone in the control variable. Background error covariance matrix $\mathbf{B}$ coming from the 1D-Var package provides variance and covariance of temperature on 54 levels (54 number being surface level), humidity in $log(kg.kg^{-1})$ on 29 levels and surface parameters (skin temperature, surface temperature and surface humidity). However this $\mathbf{B}$ matrix is not consistent with our background used in this study. Moreover, we have carried out a 1D-Var experiment including ozone in the control variable. We should therefore include ozone background standard errors $\sigma^b_{O_3}$ in addition to temperature σ^b_T, humidity $\sigma^b_{log(q)}$ and surface parameter $\left(\sigma^b_{T_{skin}}, \sigma^b_{T_{surf}}, \sigma^b_{log(q_{surf})}\right)$ errors.

To compute an appropriate background error covariance matrix $\tilde{\mathbf{B}}$, background standard errors of temperature σ^b_T and humidity $\sigma^b_{log(q)}$ are derived from the daily errors operationally used in global model ARPEGE (Berre et al., 2015), which are extracted for the same period and location as the background profiles. Cross covariances between temperature and humidity are not available in ARPEGE. However, vertical error correlations for temperature and humidity in ARPEGE are similar to those in the original $\mathbf{B}$ matrix. We can therefore compute temperature and humidity covariances and their cross covariances using multivariate temperature-humidity vertical error correlations ($\mathbf{Corr}_T$ and $\mathbf{Corr}_{log(q)}$) derived by original $\mathbf{B}$ matrix such as

$$\widetilde{\mathbf{B}}_T(i,j) = \mathbf{Corr}_T(i,j).\sqrt{\left(\sigma^b_T\right)^2_i.\left(\sigma^b_T\right)^2_j}$$

$$\widetilde{\mathbf{B}}_{log(q)}(i,j) = \mathbf{Corr}_{log(q)}(i,j).\sqrt{\left(\sigma^b_{log(q)}\right)^2_i.\left(\sigma^b_{log(q)}\right)^2_j}$$

We then computed background error covariances of ozone using $\varepsilon^b_{O_3} = \mathbf{x}^b_{O_3} - \mathbf{x}^t_{O_3}$ equation, where $\mathbf{x}^b_{O_3}$ is ozone background coming from O3MOC or O3REF and assuming that $\mathbf{x}^t_{O_3} \approx \mathbf{x}^v_{O_3}$, with $\mathbf{x}^t_{O_3}$ the unknown true state of ozone and $\mathbf{x}^v_{O_3}$ the verification data of ozone from radiosondes. We have however a limited number

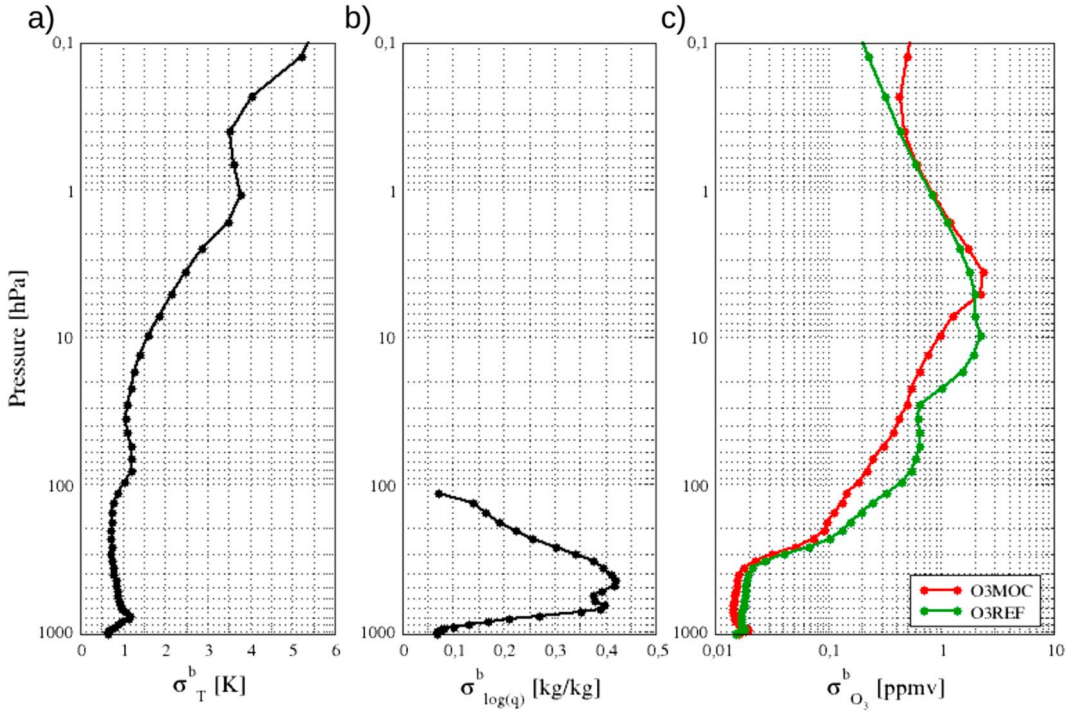

Figure 6. Temperature background standard errors σ_T^b (a), humidity background standard errors $\sigma_{log(q)}^b$ (b) and ozone background standard errors $\sigma_{O_3}^b$ for O3MOC (red line) and O3REF (green line) (c) with respect to pressure levels.

of cases and radiosondes contain errors, which can affect the range of ozone vertical covariance structures, leading to non positive matrix. We apply a compact support by multiplying vertical covariance structures by mask function:

$$mask_i(j) = \frac{1}{2}.\left[1 + cos(\pi.\frac{d_{i,j}}{D})\right] \text{ if } d_{i,j} < D; 0 \text{ otherwise}$$

where $d_{i,j}$ is the distance between pressure levels such as $d_{i,j} = |\ log(p_i) - log(p_j)\ |$ and D the maximal distance of correlation. This mask function allows the calculation of new ozone background error correlations $\widetilde{\mathbf{Corr}}_{O_3}$ and

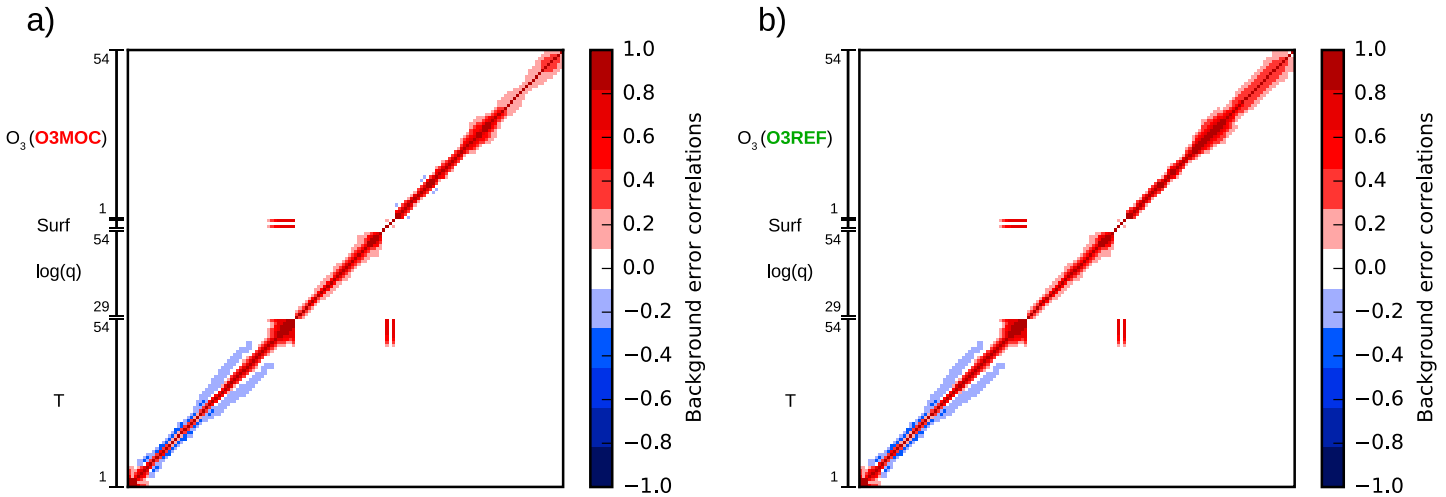

Figure 7. Background error correlations for temperature (T) on 54 vertical levels, humidity (log(q)) on 29 vertical levels, surface parameters "T_{surf}, q_{surf}, and T_{skin}" (Surf) and ozone (O_3) on 54 vertical levels from O3MOC (a) and from O3REF (b).

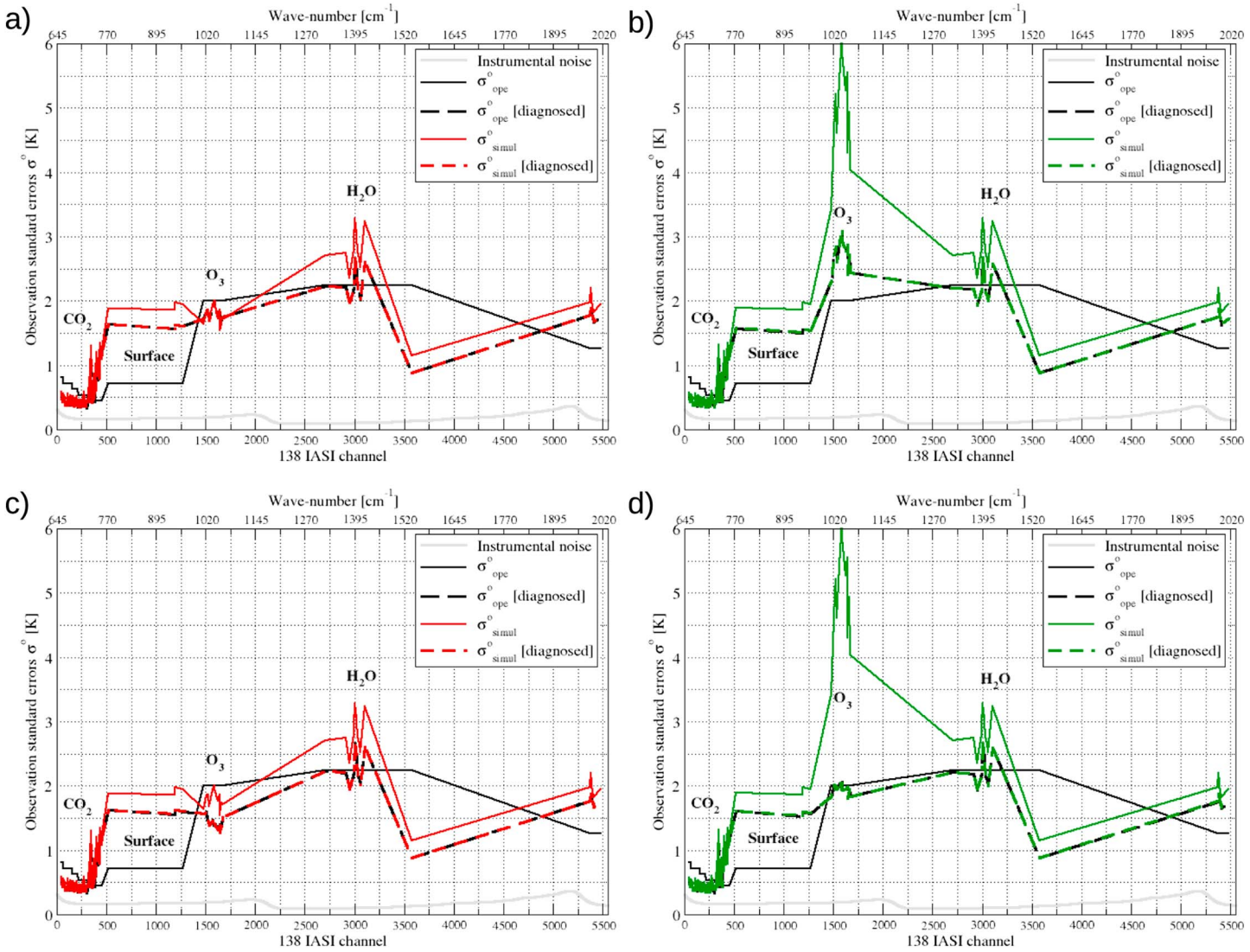

Figure 8. Operational observation errors (black line), diagnosed operational observation standard errors (black dashed), simulated observation standard errors using O3MOC (red line) (a) or O3REF (green line) (b) and diagnosed simulated observation standard errors using O3MOC (red dashed) (a) or O3REF (green line) (b) with respect to 138 IASI channels and experiments without ozone in the control variable. Operational observation standard errors (black line), diagnosed operational observation standard errors (black dashed), simulated observation standard errors using O3MOC (red line) (c) or O3REF (green line) (d) and diagnosed simulated observation standard errors using O3MOC (red dashed) (c) or O3REF (green line) (d) with respect to 138 IASI channels and experiments with ozone in the control variable.

thus ozone background error covariance matrix $\tilde{\mathbf{B}}_{O_3}$, where $\mathbf{Cov}_{O_3}$ are ozone background error covariances such as

$$\tilde{\mathbf{Corr}}_{O_3}(i,j) = \left[\frac{\mathbf{Cov}_{O_3}(i,j)}{\sqrt{\left(\sigma^b_{O_3}\right)^2_i \cdot \left(\sigma^b_{O_3}\right)^2_j}} \right] .mask_i(j)$$

$$\tilde{\mathbf{B}}_{O_3}(i,j) = \widetilde{\mathbf{Corr}}_{O_3}(i,j) . \sqrt{\left(\sigma^b_{O_3}\right)^2_i \cdot \left(\sigma^b_{O_3}\right)^2_j}$$

We obtain a full background error covariance matrix $\tilde{\mathbf{B}}$ containing variances and covariances of temperature, humidity and ozone. In this study, we have decided not to take into account cross-correlation between ozone temperature and ozone humidity. This assumption allows the feedback effects of ozone on temperature and humidity to be overcome. (Dethof & Holm, 2004).

We observe values of σ_T^b around 0.5 and 1.5 K between 1,000 and 10 hPa, then values increase up to 5.5 K at 0.1 hPa (Figure 6a). Figure 6b shows $\sigma_{log(q)}^b$ values between 0.05 and 0.45 from the surface to 100 hPa. Finally, Figure 6c shows $\sigma_{O_3}^b$ values for ozone from O3MOC on the line and ozone from O3REF on the green line. We note larger values of $\sigma_{O_3}^b$ for O3REF than O3MOC especially between 200 and 5 hPa with respect to the increase in ozone concentration. Inversely, above 5 hPa, $\sigma_{O_3}^b$ values are slightly larger for O3MOC than O3REF and more above 0.4 hPa.

Concerning temperature, the highest background error correlations are observed at the surface and in the lower troposphere (Figure 7). High background error correlations across all atmospheric columns for humidity are noted especially near the surface. A slightly higher ozone correlation for O3REF than for O3MOC is observed in the troposphere and the lower stratosphere with respect to large values of $\sigma_{O_3}^b$ for O3REF than O3MOC seen in Figure 7. In this study, the univariate ozone background covariance error matrices were chosen because calculating the cross-covariance between ozone-humidity and ozone-temperature would prove too complex in this preparatory framework.

4.3. Observation Errors

Diagonal observation-error covariance matrices only give a narrow description of the observation errors. Observation error covariances between channels however may exist, in particular due to the observation operator $\mathcal{H}$. Nevertheless, they are used in 4D-Var data assimilation for the global model ARPEGE. In our study, we have initialized the observation standard errors using values that stem from ARPEGE for the 123 operational and 15 ozone-sensitive channels $\left(\sigma_{ope}^o\right)$ (black line in Figure 8).

These observation standard errors are not adapted to our study in a 1D-Var framework however. A first step toward the estimation of realistic observation standard errors is to use standard deviation derived from the differences between IASI simulation and observation using both pieces of ozone information computed in section 3. This produces simulated observation standard errors $\left(\sigma_{simul}^o\right)$ using O3MOC (red line) or O3REF (green line) shown respectively in Figures 8a and 8c and 8b and 8d. We can see larger values of σ_{simul}^o for IASI surface sensitive channels than σ_{ope}^o. The large values of observation standard errors for surface sensitive and WV channels may be caused by cloudy cases and/or a wrong skin temperature unidentified during data filtering. The larger values of σ_{simul}^o for IASI ozone-sensitive channels simulated using O3REF are also present, compared with those simulated using O3MOC. This is a useful first approach, but these observation standard errors do not take into account the cross-correlation between channels.

In order to estimate the observation standard errors and more generally the structure of the observation error covariance matrix $\widetilde{\mathbf{R}}$, a diagnostic method introduced by (Desroziers et al., 2005) was used. Background and observation error covariance matrices can be estimated from observation departures to background and analysis. These diagnosed matrices allow the investigation of the "a priori" prescribed matrices, before analysis, are correctly specified. Taking the expected value of the cross product of $\mathbf{d}_a^o$ and $\mathbf{d}_b^o$, and using the assumption of uncorrelated errors, Desroziers et al. (2005) found a statistical approximation for the observation error covariance matrix $\tilde{\mathbf{R}}$ as mean diagnosed matrix after iterations which reads:

$$\tilde{\mathbf{R}} = \mathbf{E}\left[\mathbf{d}_a^o \left(\mathbf{d}_b^o\right)^T\right]$$

where the vector of analysis residuals $\mathbf{d}_a^o$ is the difference between observations $\mathbf{y}$ and the analysis state projected onto the observation space $\mathcal{H}(\mathbf{x}^a)$ such as $\mathbf{d}_a^o = \mathbf{y} - \mathcal{H}(\mathbf{x}^a)$ and the innovation $\mathbf{d}_b^o$. These revised matrices can be used for a new series of 1D-Var. This iterative method provides an updated version of the observation error covariance matrix $\widetilde{\mathbf{R}}$ with diagnosed observation standard errors. A set of 10 diagnostic iterations has been carried out. The updated $\widetilde{\mathbf{R}}$ matrix allows the calculation of a new analysis $\widetilde{\mathbf{x}^a}$. Desroziers diagnostic is commonly used by the assimilation community, at the MetOffice (Weston et al., 2014), and at the ECMWF (Bormann et al., 2011).

In Figure 8, we observe a decrease of diagnosed observation standard errors for surface-sensitive, ozone-sensitive and WV channels compared to simulated observation standard errors. We note a difference between diagnosed observation standard errors for ozone-sensitive channels with or without ozone in the control variable. Indeed, in Figure 8c, diagnosed observation standard errors for ozone-sensitive channels with ozone in the control variable are lower around 0.5 K than those without ozone in the control variable in Figure 8a. Also, in Figure 8d, diagnosed observation standard errors for ozone-sensitive channels with ozone in the control variable are lower around 1 K than those without ozone in the control variable in Figure 8b.

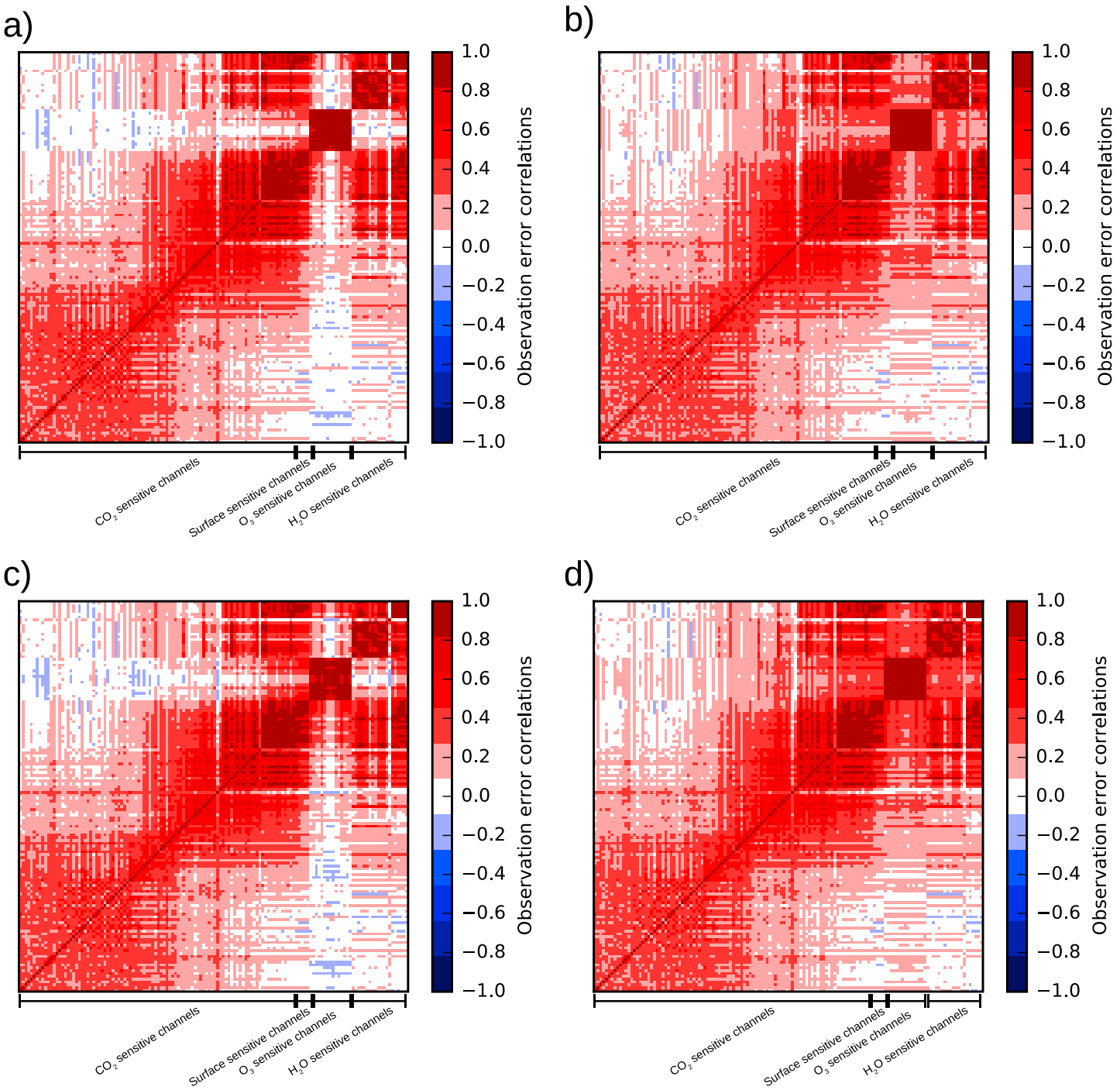

Figure 9. Observation error correlation for diagnosed observation standard error derived from σ^o_{simul} respectively using ozone information from O3MOC (a) and O3REF (b) without ozone in the control variable and observation error correlation for diagnosed observation standard error derived from σ^o_{simul} respectively using ozone information from O3MOC (c) and O3REF (d) with ozone in the control variable with respect to 138 IASI channels.

As ozone profiles are modified during 1D-Var with ozone in the control variable, this may help to better characterize the observation errors in the Desroziers method. Despite differences between σ^o_{ope} and σ^o_{simul} to diagnosed observation standard error, it is comforting to converge toward the same values. To this end, we have used diagnosed observation error covariance matrix for 1D-Var experiments. Finally, Figure 9 describes the cross-correlation between 138 IASI channels. We observe larger cross-correlations between ozone sensitive channels and other channels using O3REF than O3MOC. Figure 9c and d shows diagnosed observation

Table 2
Summary of 1D-Var Assimilation Experiments

Experiments	$\mathbf{x}^b_{O_3}$	Observation error	Background error	IASI channels assimilated
123-MOC	O3MOC	$\widetilde{\mathbf{R}}$ initialized by σ^o_{simul} for O3MOC	$\widetilde{\mathbf{B}}$ with $\sigma^b_{O_3}$ for O3MOC	123
123-REF	O3REF	$\widetilde{\mathbf{R}}$ initialized by σ^o_{simul} for O3REF	$\widetilde{\mathbf{B}}$ with $\sigma^b_{O_3}$ for O3REF	123
138-MOC	O3MOC	$\widetilde{\mathbf{R}}$ initialized by σ^o_{simul} for O3MOC	$\widetilde{\mathbf{B}}$ with $\sigma^b_{O_3}$ for O3MOC	123 +15 O_3
138-REF	O3REF	$\widetilde{\mathbf{R}}$ initialized by σ^o_{simul} for O3REF	$\widetilde{\mathbf{B}}$ with $\sigma^b_{O_3}$ for O3REF	123 + 15 O_3

standard error derived by σ^o_{simul} respectively using ozone information from O3MOC and O3REF with ozone in the control variable. Observation error correlation is sightly larger with ozone in the control variable than without.

4.4. Scores for Retrieval Evaluation

To evaluate the impact of IASI ozone sensitive channels on retrievals, 1D-Var experiments have been run for 123 IASI operational channels and 123 +15 IASI ozone-sensitive channels with ozone information derived from O3MOC or O3REF, after which two pairs of experiments remain. Investigations were conducted within a simplified framework such as the one-dimensional variational data assimilation. Indeed, 1D-Var is a common method used in research because of its low computing cost. Here, data assimilation experiments include ozone in the control variable, in addition to temperature, humidity and surface parameters. Diagnosed observation error covariance matrix $\widetilde{\mathbf{R}}$ and background error covariance matrix $\widetilde{\mathbf{B}}$ previously established were used. The experimental setting is summarized in Table 2.

To evaluate improvement of analysis (temperature, humidity and ozone retrievals), we calculated the sum of relative error reductions (REDs) of retrievals compared to background with respect to radiosonde for temperature (RED_T), humidity (RED_q), and ozone (RED_{O_3}) for 161 profiles. Evaluation criteria are crucial for the assessing of the quality impact on retrieved thermodynamic and chemical profiles. These criteria are calculated according to the formula:

$$RED_T = \sum_{i=1}^{n_T}\left[\frac{sd\left(\mathbf{x}^b_{T_i}-\mathbf{x}^v_{T_i}\right)-sd\left(\widetilde{\mathbf{x}}^a_{T_i}-\mathbf{x}^v_{T_i}\right)}{sd\left(\mathbf{x}^b_{T_i}-\mathbf{x}^v_{T_i}\right)}\right]$$

$$RED_q = \sum_{i=1}^{n_q}\left[\frac{sd\left(\mathbf{x}^b_{q_i}-\mathbf{x}^v_{q_i}\right)-sd\left(\widetilde{\mathbf{x}}^a_{q_i}-\mathbf{x}^v_{q_i}\right)}{sd\left(\mathbf{x}^b_{q_i}-\mathbf{x}^v_{q_i}\right)}\right]$$

$$RED_{O_3} = \sum_{i=1}^{n_{O_3}}\left[\frac{sd\left(\mathbf{x}^b_{O_3 i}-\mathbf{x}^v_{O_3 i}\right)-sd\left(\widetilde{\mathbf{x}}^a_{O_3 i}-\mathbf{x}^v_{O_3 i}\right)}{sd\left(\mathbf{x}^b_{O_3 i}-\mathbf{x}^v_{O_3 i}\right)}\right]$$

Using the standard deviation (*sd*), at each vertical level i, n_T and n_{O_3} being the number of 54 vertical temperature and ozone levels and n_q being the number of 29 vertical levels for humidity, $\widetilde{\mathbf{x}}^a_i$ the retrieval using diagnosed $\widetilde{\mathbf{R}}$ matrix and $\mathbf{x}^b_i$ the background minus $\mathbf{x}^v_i$ the verification data from radiosondes.

In addition, in order to quantify the information of 15 IASI ozone-sensitive channels to retrievals, we calculated the DFS (Degree of Freedom for Signal) for temperature, humidity and ozone with respect to pressure levels. Indeed, DFS provides a measure of the gain in information gathered by the observations (Rodgers, 2000) (Fisher, 2003). Here, DFS is calculated with the background error covariance matrix $\widetilde{\mathbf{B}}$ and the analysis error covariance matrix $\mathbf{A}$. $DFS = Tr(\mathbf{I} - \mathbf{A}\widetilde{\mathbf{B}}^{-1})$, where Tr is the trace of matrix.

5. Results of 1D-Var Assimilation

5.1. Evaluation in the Observation Space

The impact of adding 15 IASI ozone-sensitive channels including the ozone in the control variable of the 1D-Var is evaluated. First, we can calculate the difference between IASI observations and simulations from the retrieved profiles, $\mathbf{d}^o_a$ or (O-A) here after. We observe for 123-MOC and 123-REF experiments where whichever

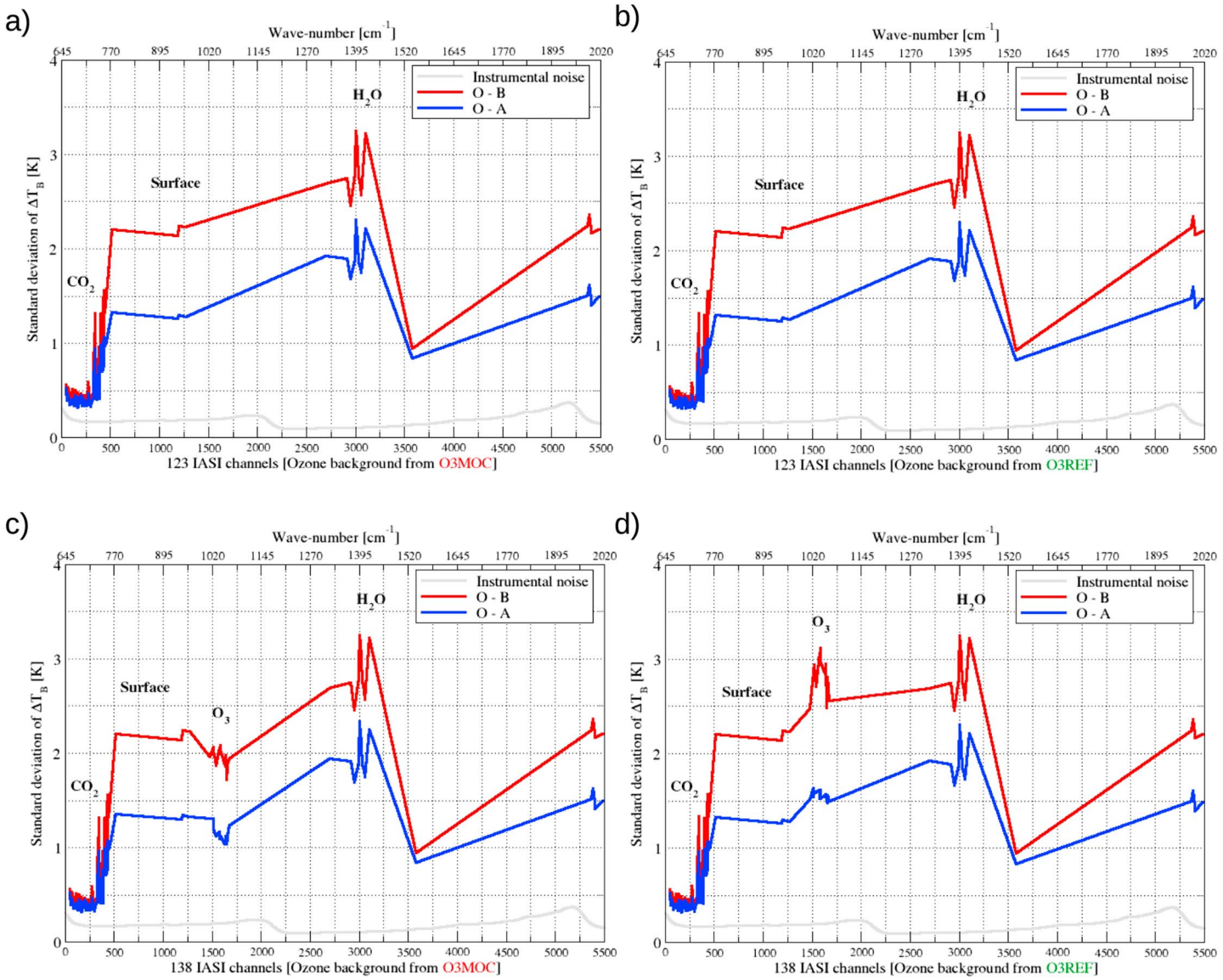

Figure 10. Standard deviation of the innovations (O-B) in red line and analysis residuals (O-A) in blue line for 123-MOC (a) and 123-REF (b) experiments with respect 123 IASI operational channels and for 138-MOC (c) and 138-REF (d) experiments with respect 123 + 15 IASI ozone-sensitive channels.

ozone background used, we obtain similar values between Figures 10a and 10b. Standard deviation of (O-A) are much lower when compared to standard deviation of [O-B] especially for surface-sensitive and WV sensitive IASI channels. These results were expected and indicated that the assimilation process works. We then added 15 IASI ozone-sensitive channels in 138-MOC and 138-REF experiments. Between Figure 10c and 10d, we can note a difference between standard deviation of [O-B] for 138-MOC and 138-REF experiments around 1 K. However, the difference between standard deviation of (O-A) for 138-MOC and 138-REF is around 0.5 K. Differences between statistics of 138-MOC and 138-REF are lower after the 1D-Var than before, which seems to indicate that ozone retrievals are closer to each other than to ozone background. These results shows that an inaccurate representation of the state vector in the ozone background, affects the posterior state.

5.2. Evaluation of the Analysis Standard Errors

Figure 11a and b, show the reduction of temperature, humidity and ozone analysis standard errors (σ^a) for (123-MOC/REF) and (138-MOC/REF) experiments compared to background standard errors. The former are lower than the latter, as 1D-Var attempts to minimize the error variance. Very few differences are observed for σ^a of temperature and humidity between (123-MOC/REF) and (138-MOC/REF) experiments. We note that σ^a of temperature and humidity from 138-MOC experiments are 1% smaller than 138-REF in the troposphere

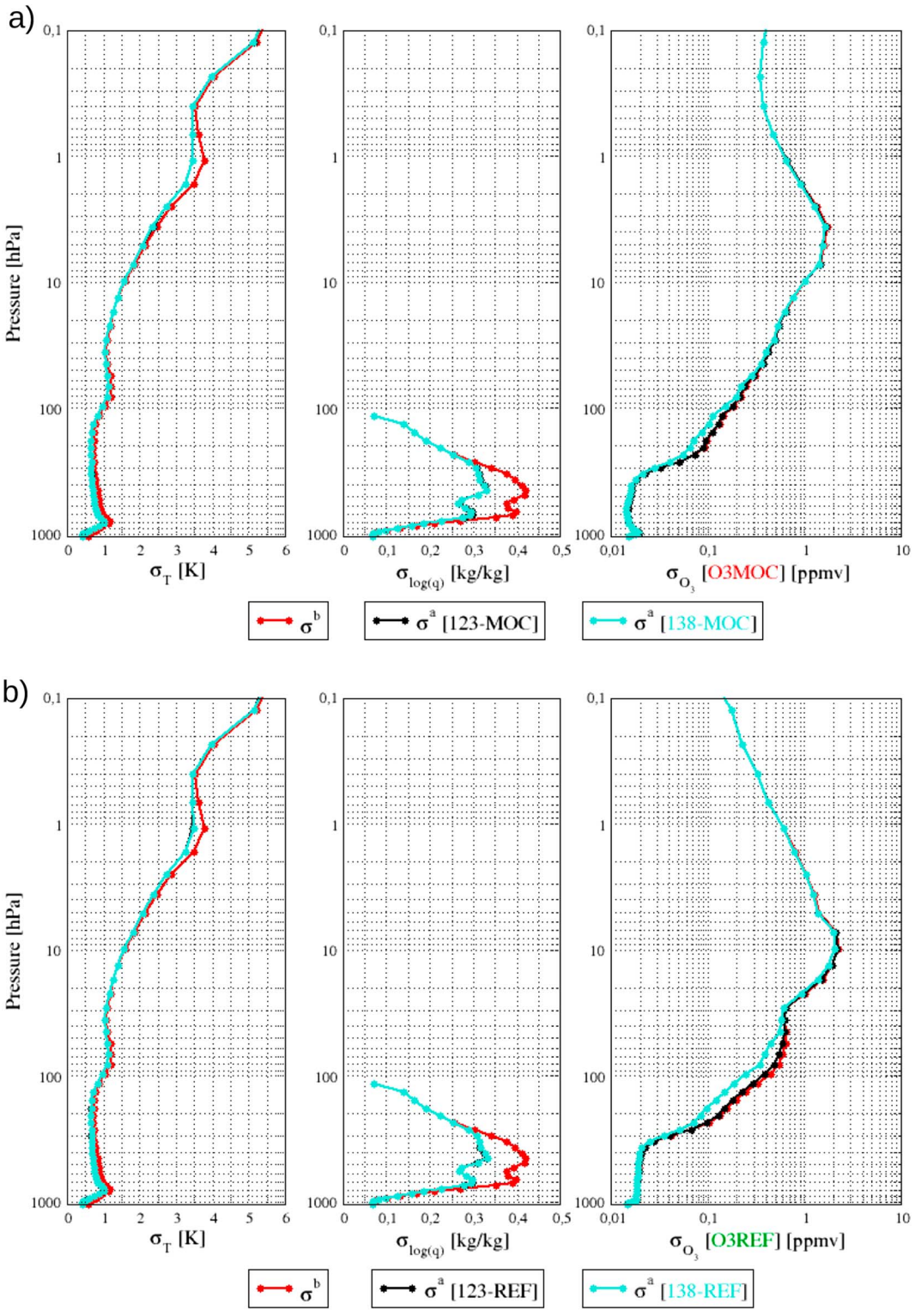

Figure 11. Background σ^b (in red line) and analysis σ^a standard errors of temperature σ_T, humidity $\sigma_{log(q)}$ and ozone σ_{O_3} for (123-MOC on the black line and 138-MOC in turquoise line) (a) and (123-REF on the black line and 138-REF on the turquoise line) (b) experiments with respect to pressure levels.

Table 3
Summary of the Results for Sum of Relative Error Reduction and DFS Averaged Over Vertical Levels for 123-MOC/REF and 138-MOC/REF Experiments

	Error reduction			Degree of Freedom for Signal		
Experiments	RED_T (%)	RED_q (%)	RED_{O_3} (%)	DFS_T	DFS_q	DFS_{O_3}
123-MOC	2.82	6.22	−0.34	4.07	2.45	0.14
138-MOC	2.87	6.44	2.79	4.12	2.49	1.54
123-REF	2.73	6.22	0	4.06	2.45	0.43
138-REF	3.03	6.70	3.34	3.96	2.41	1.96

between 700 and 300 hPa. We note a better reduction for σ^a of humidity from the 138-MOC experiment than from 138-REF. Obviously, a larger reduction of analysis standard errors are obtained for ozone. We observe a slight difference between σ^b and σ^a of ozone for 123-MOC/REF experiments. Reduction of σ^a for ozone from 138-MOC/REF experiments compared to 123-MOC/REF is more important for 138-REF, between 300 and 30 hPa because σ^b of ozone from O3REF are larger than O3MOC and thus, ozone analysis of O3REF can differ more from the background. This location is consistent with ozone Jacobians as we have seen in Figure 1c. However, σ^a of ozone from the 138-MOC experiment are 20% smaller than 138-REF in the troposphere between 700 and 300 hPa and 40% in the stratosphere between 100 and 10 hPa. As some IASI CO_2 sensitive channels are also sensitive to ozone, they can also modify the ozone profile during the 1D-Var.

5.3. Evaluation of the Retrievals

Hereafter, positive values of error reduction (RED) mean that retrievals from 123-MOC/REF or 138-MOC/REF are better than background. Conversely, negative values mean that retrievals are worse than background. The results of RED and DFS are averaged over vertical levels for experiments and summarized in Table 3. Assessments of temperature, humidity and ozone retrieval biases compared to background biases using SONDE as verification for our experiments shows no significant differences (not shown).

• Impact on temperature

In Figure 12a very few differences are observed for RED_T vertical profiles between 123-MOC and 138-MOC, with a 0.05% increase for RED_T in 138-MOC compared to 123-MOC. Improvement comes through using ozone background from O3REF in Figure 12b with a 0.30% increase for RED_T in 138-REF compared to 123-REF. The values of DFS_T for 123-MOC and 123-REF experiments are similar. DFS_T is slightly higher for the 138-MOC experiment (4.12) than the 138-REF (3.96) indicating a better use of IASI ozone-sensitive channels with ozone background from O3MOC to improve temperature retrievals.

• Impact on humidity

RED_q vertical profiles show no differences for experiments between 123-MOC in Figure 12c and 123-REF in Figure 12d. Improvement for humidity is greater than for temperatures with a 0.22% increase for RED_q in 138-MOC compared to 123-MOC and 0.48% for 138-REF compared to 123-REF. These improvements of RED_q vertical profiles provided by 15 IASI ozone-sensitive channels in 138-MOC/REF experiments are located between 1,000–800 hPa and 400–100 hPa. Results are consistent with humidity Jacobians of these channels (see Figure 1b). Similar, values of DFS_q for 123-MOC and 123-REF experiments are observed. DFS_q is slightly greater for the 138-MOC experiment (2.49) than the 138-REF (2.41) indicating a better use of IASI ozone-sensitive channels with ozone background from O3MOC in order to improve humidity retrievals.

• Impact on ozone

Without ozone-sensitive channels, RED_{O_3} vertical profiles for the 123-MOC experiment shows a degradation in Figure 12e and for 123-REF in Figure 12f. As expected, major improvements for ozone retrievals are obtained when adding 15 IASI ozone-sensitive channels in 138-MOC/REF experiments. Better improvement of RED_{O_3} is achieved this time using ozone background from O3REF with a 3.34% increase in the 138-REF experiment compared to 138-MOC and with 2.45%. Vertical level pressure of these improvements differ between 138-MOC and 138-REF with a relative improvement across all atmospheric profiles for 138-MOC. For 138-REF improvement is between 600 and 30 hPa beyond which RED_{O_3} vertical profile is degraded. DFS_{O_3} vertical profiles also differ between 138-MOC (1.54) and 138-REF (1.96). Two explanations can be suggested for the

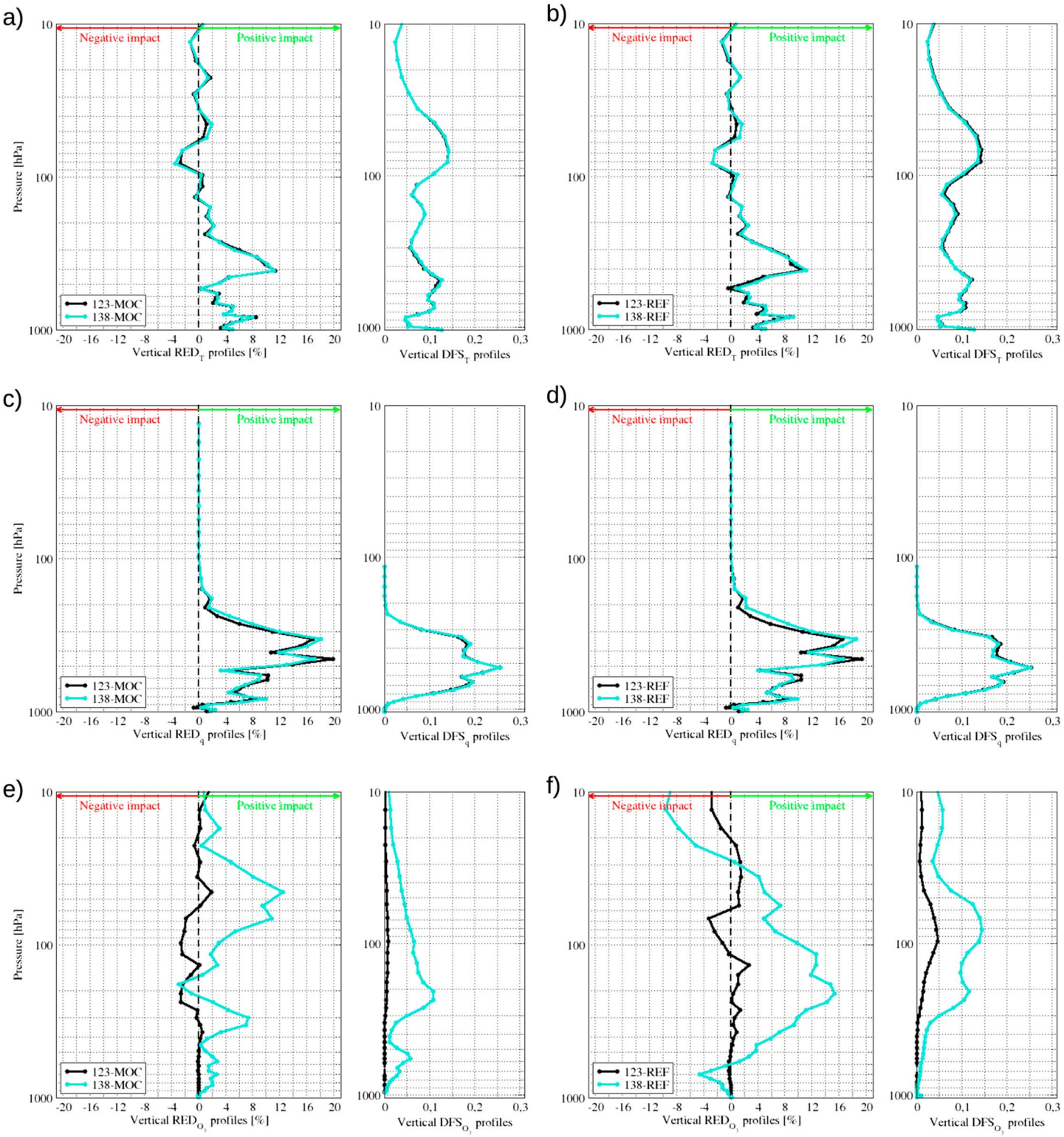

Figure 12. Vertical Degree of Freedom for Signal (DFS) and vertical RED of retrievals (123-MOC/REF on the black line and 138-MOC/REF on the turquoise line) compared to background with respect to radiosonde for temperature using ozone background from O3MOC (a) and O3REF (b), for humidity using ozone background from O3MOC (c) and O3REF (d) and for ozone using ozone background from O3MOC (e) and O3REF (f) with respect to pressure.

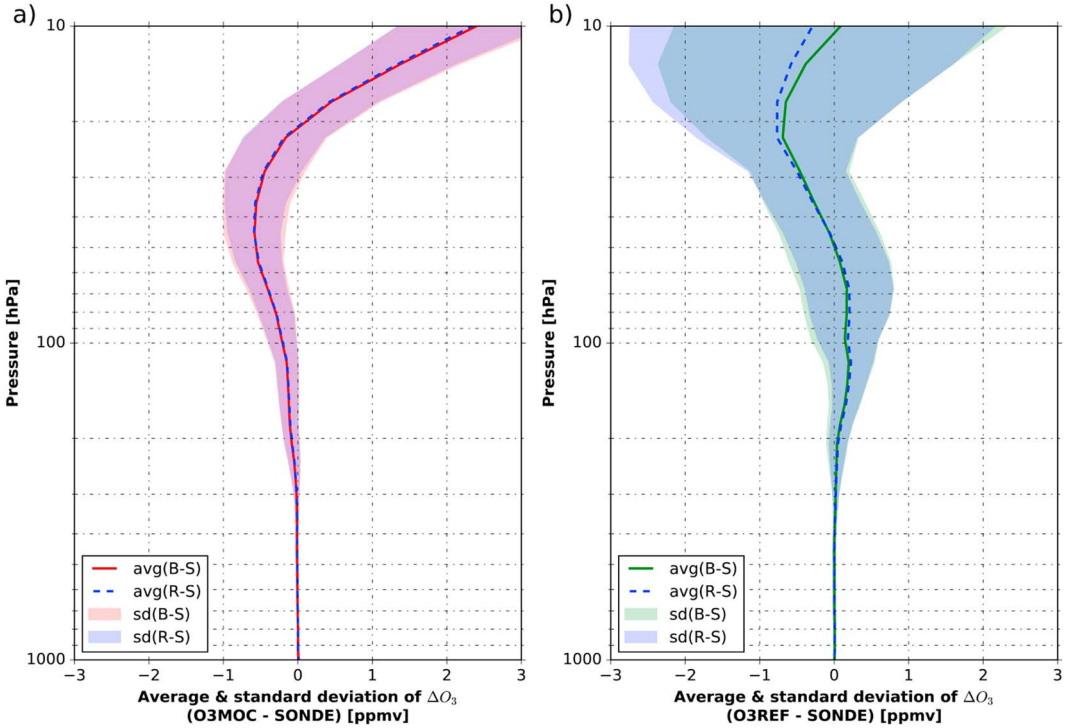

Figure 13. Average and standard deviation of differences between ozone background minus SONDE (B − S) and retrieval minus SONDE (R − S) for 138-MOC (a) and 138-REF (b) with respect to pressure.

differences. Firstly, ozone background errors of O3MOC and O3REF differ; $\widetilde{\mathbf{B}}_{O_3}$ of O3REF has larger ozone background errors than O3MOC, allowing a higher degree of freedom to adjust the O3REF ozone background. Secondly, differences between both DFS_{O_3} were also influenced by Jacobians, which vary depending on ozone background.

Finally, we can evaluate ozone retrievals that come from 138-MOC/REF directly against SONDE. Figure 13 shows average and standard deviation of differences between ozone retrievals and SONDE using ozone background that comes from O3MOC (a) or O3REF (b) in addition to similar statistics between ozone background and SONDE shown in Figure 4 (section 2.3.2). (B − S) means background minus SONDE for ozone from O3MOC (red line) and O3REF (green line). (R − S) means retrieval minus SONDE ozone background (O3MOC (a) or O3REF (b)) and SONDE (blue pulled). In Figure 13a, biases of (R − S) are close to biases of (B − S), and better between 20 and 10 hPa. In addition, standard deviations of (R − S) are generally smaller compared to standard deviations of (B − S) over the entire atmospheric column. While on Figure 13b for O3REF, biases of (R − S) are not as accurate good as biases of (B − S) from the surface to 10 hPa. Standard deviations of (R − S) are smaller than standard deviations of (B − S) from surface to 30 hPa and larger between 30 and 10 hPa. Thus, standard deviation of (R − S) using O3MOC is 40% smaller than standard deviation of (R − S) using O3REF from surface to 200 hPa, 60% between 200 and 30 hPa and 65% between 30 and 10 hPa. These results confirm that ozone which originates from O3MOC is the best ozone background to use to improve respectively temperature, humidity, and ozone retrievals.

6. Conclusions and Discussions

This work is part of the ambition to move toward coupled data assimilation between Numerical Weather Prediction and CTM by means of infrared satellite observations. At Météo-France, the 4D-Var assimilation system in the global NWP model ARPEGE uses only 123 IASI channels out of 314 monitored. Information on atmospheric composition for the assimilation of radiances from the IASI infrared sounder uses concentrations of some gases that vary neither in time nor in space. In this study, a simplified framework is used: 15 IASI ozone-sensitive channels have been assimilated in a 1D-Var in addition to IASI operational channels using realistic ozone profiles, which originate from MOCAGE CTM.

A data impact study with 1D-Var analysis was conducted from April 2014 to March 2015, on 161 background profiles collocated with clear-sky IASI pixels and radiosondes. Preliminarily, both pieces of ozone information originating from MOCAGE CTM (O3MOC) and RTTOV reference profile (O3REF) were evaluated through the comparison of simulations of the IASI observations. This study has shown that the use of realistic ozone information from O3MOC input of the RTTOV RTM allows better stimulation of IASI ozone-sensitive channel radiances than the use of ozone reference from O3REF. These results were expected and take into account the spatial and temporal variability of ozone in MOCAGE CTM. Indeed, statistics of differences between both ozone information and radiosondes show a standard deviation twice the size for O3REF than O3MOC.

These are useful results for the estimation of realistic observation standard errors used as diagonal observation covariance error matrix **R** for 1D-Var assimilation processes. They are then compared to operational standard errors used in 4D-Var ARPEGE thus not adapted for our case. Filtering of 161 clear-sky cases have definitely overlooked a few cloudy cases identified by the high standard deviation of [O-B] differences of IASI surface sensitive channels however. Hence, we have calculated a new $\widetilde{\mathbf{R}}$ from Desroziers' diagnostic, which allows the estimation of realistic observation standard errors taking into account the full cross-correlation from the iterative method. To extract the maximum amount of information that comes from IASI ozone sensitive channels, we should consider ozone background standard errors. To achieve this, we have added ozone to the 1D-Var control variable and estimated a new background covariance error matrix $\widetilde{\mathbf{B}}$ including ozone errors for O3MOC or O3REF.

The impact of 15 IASI ozone sensitive channels on the analysis was evaluated with RED of temperature, humidity, and ozone analyses compared to background with respect to radiosondes and DFS. Results of 1D-Var retrievals show that besides the significant improvement of ozone analysis, IASI ozone-sensitive channels provide additional information in order to improve temperature and humidity analyses, especially as the error reduction is increasing by 2.0% between 400 and 200 hPa. What is more, ozone DFS showed that IASI ozone-sensitive channels covering the large part of the vertical atmospheric range are able to provide additional information at levels where carbon dioxide and WV sensitive channels are less sensitive. Different results using either O3MOC or O3REF are explained by ozone standard errors in $\widetilde{\mathbf{B}}$ matrix. In addition, the low number of cases (161), does not enable us to take into account realistic error variability. Assimilation of these ozone-sensitive channels allows however the substantial improvement of ozone retrievals and the increase of the error reduction by up to 11.0% for O3MOC background at 45 hPa. The main conclusion is that it is possible to improve temperature and humidity analyses of ARPEGE by adding IASI ozone-sensitive channels to in the assimilation system. This also allows us to improve ozone profiles especially at the level of atmospheric layers difficult to model by CTM.

The next step will be to use the same approach in 4D-Var ARPEGE. First of all, other IASI ozone-sensitive channels will be selected from the full IASI spectrum. Experiments show that 503 IASI channels are sensitive to ozone, composed of 18 between 714.5 and 754cm^{-1}, 314 between 989.25 and 1,081.5 cm^{-1}, and 171 between 2,071.25 and 2,131.25 cm^{-1}. Only channels in an ozone-sensitive band will be considered. Ozone will then be added to the 4D-Var ARPEGE control variable and a new ozone background covariance errors matrix will be calculated considering ozone errors using the NMC method (Jeuken et al., 1999) or an ensemble method (Massart et al., 2012) so as to calculate an ozone background covariance error matrix in near real time. Furthermore, the impact of additional ozone-sensitive channels using ozone information from MOCAGE CTM to thermodynamic forecast will be assessed.

Acknowledgments
This research has been conducted within the framework of O. Coopmann's PhD thesis, which is funded by CNES and the Région Occitanie. The authors would like to acknowledge Jean-François MAHFOUF and Jean-Antoine MAZIEJEWSKI for their help in revising and increasing the quality of the manuscript. The anonymous reviewers are thanked for previous guidance. Data of radiosondes are available through these websites: (WOUDC, available online at http://www.woudc.org; SHADOZ, available online at croc.gsfc.nasa.gov/shadoz/Archive.html, and NOAA/Earth System Research Laboratory (ESRL), and Global Monitoring Division (GMD) networks available online at ftp://ftp.cmdl.noaa.gov/ozwv/ozone/). IASI data are available from EUMETSAT or AERIS (https://www.aeris-data.fr/). Model data are available online at https://mycore.core-cloud.net/index.php/s/ZXupzclFXbCHCTb.

References

August, T., Klaes, D., Schlüssel, P., Hultberg, T., Crapeau, M., Arriaga, A., et al. (2012). IASI on Metop-A: Operational level 2 retrievals after five years in orbit. *Journal of Quantitative Spectroscopy and Radiative Transfer*, *113*(11), 1340–1371.

Berre, L., Varella, H., & Desroziers, G. (2015). Modelling of flow-dependent ensemble-based background-error correlations using a wavelet formulation in 4D-Var at météo-france. *Quarterly Journal of the Royal Meteorological Society*, *141*(692), 2803–2812.

Borbas, E. E., & Ruston, B. C. (2011). *The RTTOV UWiremis IR Land Surface Emissivity Module*. Darmstadt.: EUMETSAT.

Bormann, N., Geer, A. J., & Bauer, P. (2011). Estimates of observation-error characteristics in clear and cloudy regions for microwave imager radiances from Numerical Weather Prediction. *Quarterly Journal of the Royal Meteorological Society*, *137*(661), 2014–2023.

Bouttier, F., & Kelly, G. (2001). Observing-system experiments in the ECMWF 4D-Var data assimilation system. *Quarterly Journal of the Royal Meteorological Society*, *127*(574), 1469–1488.

Cayla, F.-R. (2001). L'interféromètre iasi-un nouveau sondeur satellitaire haute résolution.

Chevallier, F., Di Michele, S., & McNally, A. P. (2006). *Diverse Profile Datasets from the ECMWF 91-Level Short-range Forecasts*. Shinfield Park, Reading: European Centre for Medium-Range Weather Forecasts.

Clerbaux, C., Boynard, A., Clarisse, L., George, M., Hadji-Lazaro, J., Herbin, H., et al. (2009). Monitoring of atmospheric composition using the thermal infrared IASI/Metop sounder. *Atmospheric Chemistry and Physics*, *9*(16), 6041–6054.

Collard, A. (2007). Selection of IASI channels for use in Numerical Weather Prediction. *Quarterly Journal of the Royal Meteorological Society*, *133*(629), 1977–1991.
Derber, J. C., & Wu, W.-S. (1998). The use of Tovs cloud-cleared radiances in the NCEP SSI analysis system. *Monthly Weather Review*, *126*(8), 2287–2299.
Desroziers, G., Berre, L., Chapnik, B., & Poli, P. (2005). Diagnosis of observation, background and analysis-error statistics in observation space. *Quarterly Journal of the Royal Meteorological Society*, *131*(613), 3385–3396.
Dethof, A., & Holm, E. (2004). Ozone assimilation in the era-40 reanalysis project. *Quarterly Journal of the Royal Meteorological Society*, *130*(603), 2851–2872.
Donlon, C. J., Martin, M., Stark, J., Roberts-Jones, J., Fiedler, E., & Wimmer, W. (2012). The operational sea surface temperature and sea ice analysis (ostia) system. *Remote Sensing of Environment*, *116*, 140–158.
Dragani, R., & McNally, A. (2013). Operational assimilation of ozone-sensitive infrared radiances at ECMWF. *Quarterly Journal of the Royal Meteorological Society*, *139*, 2068–2080.
Fisher, M. (2003). *Estimation of Entropy Reduction and Degrees of Freedom for Signal for Large Variational Analysis Systems*. Shinfield Park, Reading: European Centre for Medium-Range Weather Forecasts.
Guedj, S., Karbou, F., & Rabier, F. (2011). Land surface temperature estimation to improve the assimilation of Seviri radiances over land. *Journal of Geophysical Research*, *116*, D14107. https://doi.org/10.1029/2011JD015776
Han, W., & McNally, A. (2010). The 4D-Var assimilation of ozone-sensitive infrared radiances measured by iasi. *Quarterly Journal of the Royal Meteorological Society*, *136*, 2025–2037.
Hilton, F., Antonelli, P., Calbet, X., Hultberg, T., Lavanant, L., Liu, X., et al. (2009). An investigation into the performance of retrievals of temperature and humidity from iasi.
Hilton, F., Armante, R., August, T., Barnet, C., Bouchard, A., Camy-Peyret, C., et al. (2012). Hyperspectral Earth observation from IASI: Five years of accomplishments. *bulletin of the american meteorological Society*, *93*(3), 347–370.
Jeuken, A., Eskes, H., Velthoven, P. v., Kelder, H., & Hólm, E. (1999). Assimilation of total ozone satellite measurements in a three-dimensional tracer transport model. *Journal of Geophysical Research*, *104*(D5), 5551–5563.
Lorenc, A. C., & Marriott, R. T. (2014). Forecast sensitivity to observations in the met office global Numerical Weather Prediction system. *Quarterly Journal of the Royal Meteorological Society*, *140*(678), 209–224.
Lupu, C., & McNally, A. P. (2013). *Wind tracing with ozone-sensitive radiances from SEVIRI*. Shinfield Park, Reading: European Centre for Medium-Range Weather Forecasts.
Martinet, P., Lavanant, L., Fourrié, N., Rabier, F., & Gambacorta, A. (2014). Evaluation of a revised IASI channel selection for cloudy retrievals with a focus on the Mediterranean basin. *Quarterly Journal of the Royal Meteorological Society*, *140*(682), 1563–1577.
Massart, S., Piacentini, A., & Pannekoucke, O. (2012). Importance of using ensemble estimated background error covariances for the quality of atmospheric ozone analyses. *Quarterly Journal of the Royal Meteorological Society*, *138*(665), 889–905.
Matricardi, M. (2008). *The Generation of RTTOV Regression Coefficients for IASI and AIRS Using a New Profile Training Set and a New Line-by-line Database*. Shinfield Park, Reading: European Centre for Medium-Range Weather Forecasts.
Pougatchev, N., August, T., Calbet, X., Hultberg, T., Oduleye, O., Schlüssel, P., et al. (2009). IASI temperature and water vapor retrievals — Error assessment and validation. *Atmospheric Chemistry and Physics*, *9*(17), 6453–6458.
Rodgers, C. D. (2000). *Inverse Methods for Atmospheric Sounding: Theory and Practice* (Vol. 2). Singapore: World Scientific.
Saunders, R. W., & Kriebel, K. T. (1988). An improved method for detecting clear sky and cloudy radiances from avhrr data. *International Journal of Remote Sensing*, *9*(1), 123–150.
Saunders, R., Matricardi, M., & Brunel, P. (1999). An improved fast Radiative Transfer Model for assimilation of satellite radiance observations. *Quarterly Journal of the Royal Meteorological Society*, *125*(556), 1407–1425.
Semane, N., Peuch, V.-H., Pradier, S., Desroziers, G., Amraoui, L. E., Brousseau, P., et al. (2009). On the extraction of wind information from the assimilation of ozone profiles in météo–france 4-D-Var operational NWP suite. *Atmospheric Chemistry and Physics*, *9*(14), 4855–4867.
Sherlock, V., & Saunders, R. (1999). ISEM-6: Infrared surface emissivity model for rttov-6 (*NWP-SAF report*), Bracknell.
Sic, B., El Amraoui, L., Marécal, V., Josse, B., Arteta, J., Guth, J., et al. (2015). Modelling of primary aerosols in the chemical transport model MOCAGE: Development and evaluation of aerosol physical parameterizations. *Geoscientific Model Development*, *8*(2), 381–408.
Weston, P., Bell, W., & Eyre, J. (2014). Accounting for correlated error in the assimilation of high-resolution sounder data. *Quarterly Journal of the Royal Meteorological Society*, *140*(685), 2420–2429.